Scour Forecasting for Offshore Wind Parks

Hartvig, Peres Akrawi

Publication date:
2011

Document Version
Publisher's PDF, also known as Version of record

Scour Forecasting For Offshore Wind Parks

Scour Forecasting For Offshore Wind Parks

PhD Thesis

Peres Akrawi Hartvig

AALBORG UNIVERSITY
Department of Civil Engineering

ISSN 1901-7294
DCE Thesis No. 30

Aalborg University
Department of Civil Engineering
Division of Water & Soil

DCE Thesis No. 30

Scour Forecasting For Offshore Wind Parks

Thesis defended in public on 12 December 2011
at Aalborg University Esbjerg

by

Peres Akrawi Hartvig

September 2011

Scientific Publications at the Department of Civil Engineering

Technical Reports are published for timely dissemination of research results and scientific work carried out at the Department of Civil Engineering (DCE) at Aalborg University. This medium allows publication of more detailed explanations and results than typically allowed in scientific journals.

Technical Memoranda are produced to enable the preliminary dissemination of scientific work by the personnel of the DCE where such release is deemed to be appropriate. Documents of this kind may be incomplete or temporary versions of papersor part of continuing work. This should be kept in mind when references are given to publications of this kind.

Contract Reports are produced to report scientific work carried out under contract. Publications of this kind contain confidential matter and are reserved for the sponsors and the DCE. Therefore, Contract Reports are generally not available for public circulation.

Lecture Notes contain material produced by the lecturers at the DCE for educational purposes. This may be scientific notes, lecture books, example problems or manuals for laboratory work, or computer programs developed at the DCE.

Theses are monograms or collections of papers published to report the scientific work carried out at the DCE to obtain a degree as either PhD or Doctor of Technology. The thesis is publicly available after the defence of the degree.

Latest News is published to enable rapid communication of information about scientific work carried out at the DCE. This includes the status of research projects, developments in the laboratories, information about collaborative work and recent research results.

Published 2011 by
Aalborg University
Department of Civil Engineering
Sohngaardsholmsvej 57
DK-9000 Aalborg, Denmark

Printed in Esbjerg

ISSN 1901-7294
DCE Thesis No. 30
Keywords: scour, backfilling, time development, monopile

Summary

In an effort to minimize the costs of offshore wind parks, the present research deals with optimizing a certain aspect of the support structure, namely the approach to scour. Scour is the phenomenon of seabed changes in the vicinity of the support structure that arises when the support structure disturbs the local flow sufficiently much. Scour is particularly evasive because in case of current, the flow disturbance can be intense and dig a hole *comparable to the horizontal extent of the support structure*. This usually implies a considerable loss of stiffness, ultimate strength or lifetime of the support and super structure. In case of waves, however, the flow disturbance can be much weaker and even backfill the hole with soil. The ability to accurately forecast this development of the geometry of the scour hole becomes central for obtaining both a safe and cost-effective solution. In practice, scour forecasts facilitate the comparison between a scour design based on either deployment of scour-protection or enhanced structural design.

The broad goal is to *develop a method that produces accurate scour forecasts for offshore wind parks*. The present research investigates more specifically *which* parameters are suitable for characterizing the scour geometry during both scouring and backfilling and *how the parameters develop in time* for a given sea state. The present research is restricted to treat a monopile in sand since this is a common and potentially cost-saving case. The research leaves behind two legacies that deal with these two research questions in dialectical ways.

The first legacy is a framework for the scour geometry based on epistemological considerations, theoretical concepts and model-

scale experiments. Relevant parameters are reviewed, defined and discussed. The combined use of the depth and the volume of the scour hole is recommended for characterizing the scour geometry and a scour shape factor is introduced to couple them together. Simple ordinary differential equations are reviewed and compared to the experiments and one set of equations involving the scour volume and the scour shape factor are found to fit excellent with the experiments. The present findings entail some degree of departure from the traditional focus in scouring research that only considers the depth of the hole.

The second legacy is the reverse approach. This is a theoretical and numerical approach under development that relates the scour geometry development to the flow intensity. The aim of introducing the approach is to provide a supplementary way for estimating the parameter values for the mentioned equations. The reverse approach is detailed, discussed, compared to other studies and found to be in need of some improvement.

The two legacies rely on a too limited basis to reach the broad goal of developing accurate scour forecasts. However, both legacies are thought to be novel and valuable contributions to the research community towards reaching it.

* * *

Resumé

For at reducere udgifterne i forbindelse med havvindmølleparker fokuserer denne forskningsindsats på et særligt aspekt ved fundamentet, nemlig tilgangen til scour. Scour er det fænomen, der opstår, når fundamentet forårsager en så stor forstyrrelse af den lokale strømning, at havbunden omkring fundamentet ændrer sig. Scour er særlig svært at behandle fordi strømningsforstyrrelsen dels kan være intens ved påvirkning fra havstrøm og grave et hul *svarende til den vandrette udbredelse af fundamentet*. Dette medfører sædvanligvis et betydeligt tab af styrke, stivhed eller levetid for fundamentet og møllen. Dels kan strømningsforstyrrelsen være meget svagere ved påvirkning af havbølger og endda fylde hullet op igen med jord. Evnen til at kunne forudsige denne udvikling af hullets geometri bliver dermed central for at sikre både en teknisk og økonomisk bæredygtig løsning. I praksis kan scourprognoserne danne baggrund for en sammenligning mellem et scourdesign baseret på scourbeskyttelse eller forstærket konstruktionsdesign.

Det overordnede mål er at *udvikle en metode til at lave sikre scourprognoser for havvindmøller.* Denne forskningsindsats undersøger mere konkret *hvilke* parametre, der er egnede til at karakterisere hullets geometri under både udgravning og opfyldning, samt *hvordan parametrene udvikler sig over tid* for en given havtilstand. Der afgrænses til at behandle en monopæl i sand da dette tilfælde ofte forekommer og ser ud til at kunne optimeres. Forskningsindsatsen efterlader to bidrag, som behandler disse to spørgsmål på dialektisk vis.

Det første bidrag er en metodisk ramme for geometrien af hullet baseret på epistomologiske overvejelser, teoretiske koncepter og

forsøg i modelskala. Relevante parametre er gennemgået, defineret og diskuteret. Det anbefales at karakterisere hullet med dybden og rumfanget tilsammen og en formfaktor introduceres til at relatere disse til hinanden. Simple ordinære differentialligninger er gennemgået og sammenlignet med forsøgene og et sæt ligninger, der tager udgangspunkt i hullets rumfang og formfaktor, beskriver forsøgene meget tilfredsstillende. Disse resultater indikerer en vis forskydning væk fra det traditionelle fokus indenfor videnskaben om scour, som kun betragter hullets dybde.

Det andet bidrag er den omvendte metode. Dette er en teoretisk og numerisk metode under udvikling, som relaterer hullets geometriske udvikling til strømningens intensitet. Målet med at introducere metoden er at udbyde en supplerende måde hvorpå parameterværdierne for de omtalte ligninger kan skønnes. Den omvendte metode er beskrevet, diskuteret, sammenlignet med andre undersøgelser og vurderet til at skulle forbedres yderligere.

De to bidrag hviler på et for beskedent grundlag til at kunne opnå det overordnede mål om at udvikle sikre scourprognoser. Men begge bidrag vurderes at være nytænkende og værdifulde bidrag til forskningsmiljøet i bestræbelserne på at nå målet.

* * *

Preface

This thesis, *Scour forecasting for offshore wind parks*, is submitted in partial fulfillment of the requirements for obtaining the degree Doctor of Philosophy. The work was carried out from 1 August 2008 to 2 October 2011 at the Department of Civil Engineering, Aalborg University, Denmark. The thesis was defended on 12 December 2011 at Aalborg University Esbjerg.

The project went under the title *Time Development of Scour Around Offshore Monopiles* and was financed jointly by the Danish state, Dong Energy and Aalborg University. The main supervision was carried out by Head of Department Peter Frigaard and assisted by associate professor Thomas Lykke Andersen.

The project consists of the present thesis and a collection of five references:

- *Ref. 1(a):* Peres Akrawi Hartvig, Jess McCann Thomsen, Peter Frigaard, and Thomas Lykke Andersen. Experimental study of the development of scour & backfilling. *Coastal Eng. J.*, 52 (2):157–194, 2010. doi: 10.1142/S0578563410002154. Postprint available at vbn.aau.dk.
- *Ref. 1(b):* Peres Akrawi Hartvig, Jess McCann Thomsen, Peter Frigaard, and Thomas Lykke Andersen. Full erratum for "experimental study of the development of scour & backfilling". In *DCE Technical Memorandum*, number 12. Department of Civil Eng., Aalborg University, 2011. Available at vbn.aau.dk.
- *Ref. 2:* Peres Akrawi Hartvig. New framework for geometry of transient monopile scour. Presentation at 3rd workshop on

Seabed Windfarm Interaction, November 2010.

- *Ref. 3:* Peres Akrawi Hartvig. Model for the evolving bed surface around an offshore monopile. In review, 2011a.
- *Ref. 4:* Peres Akrawi Hartvig. The reverse approach for monopile scour. Submitted, 2011b.

Thank yous I wish to thank the financers, the doctoral school and the department for sponsoring and facilitating a learningful and thoughtful journey into the realms of international research and domestic work-life. I thank my primary supervisor, Peter Frigaard, for his attitude of equality, generous trust and for sharing his network of contacts with me. Thanks also to my earlier office mate Jorge Robert Rodriguez Ramirez for the experiences that we have shared together. Thanks to Henrik Stensgaard Toft and Lasse Gilling for offering an open door and mentoring during the process.

In connection with my first paper, thanks to Jess McCann Thomsen for making his experimental data available and taking the time to answer my many questions. Thanks to Thomas Lykke Andersen and Figen Hatipoglu Dixen for giving critical comments.

I also thank the staff at Institute of Energy Systems at Edinburgh University where I was visiting researcher during autumn 2009. Special thanks to Pauline Clark for arranging housing, David Ingram for offering local supervision and Mathew Topper and Eoghan Maguire for discussions on wave simulations. Finally, a big thanks to David Forehand, Ally Price and others for taking Susanne and I along to the highlands on an unforgettable journey. Returning to Denmark, I wish to thank my new colleagues at Aalborg University in Esbjerg for a warm welcome after I arrived at autumn 2011.

Finally, I thank my wife, Susanne, for sharing both the joys and burdens related to this work during these past three years.

* * *

Contents

Thesis Outline

In this section, I give a brief overview of the structure of this thesis. The first part of the thesis, *Presentation*, is divided into the following six chapters:

- *Chap. 1: Context.* A general introduction to offshore wind parks, support structures and typical ways to account for scour is given.
- *Chap. 2: Aims.* The aims and bounds of this research are stated and related to the presented context.
- *Chap. 3: Review of Scour.* A focused review of existing research on the flow and the scour around a monopile in sand is presented.
- *Chap. 4: Legacy I: Framework for Scour Geometry.* The first contribution of this research is presented.
- *Chap. 5: Legacy II: The Reverse Approach.* The second contribution is presented.
- *Chap. 6: Conclusions & Future work.* The conclusions from the two contributions and suggestions for future work are recapped.

Throughout these chapters, I make use of examples that are central for the arguments of the main text but can be read independently. Notes are denoted with superscript numbers and are listed at the end of the presentation under the respective chapter in which they appeared. Then follows the bibliography with a list of the employed literature. The second part of the thesis, *References*, contains the collection of papers, except Ref. 2.

Part I

Presentation

Chapter 1

Context

In this chapter, I give a general description of the context in which this research is embedded since this will steer the aims of the research. In the first two sections, I describe the potentials and challenges of offshore wind parks and outline three common support structures. In the last section, I focus on scour and exemplify different ways to cope with scour.

1.1 Offshore wind parks

In the recent years, there has been an increased interest in *offshore wind parks* as a source of renewable energy. I have collected some notable onshore and offshore wind parks in Table 1.1 where the reported records are held at the time as I write.

Compared to the onshore ones, the offshore wind parks usually enjoy at least three advantages of political and technical nature:

- *Lower visual and audial impact.* This is due to the typically increased distance between the park and the observers as illustrated in Fig. 1.1.
- *Plentier availability of unused and large space.*
- *Stronger and steadier power output.* This is partly due to the stronger and steadier wind at sea and the space availability that allows a large cluster of wind turbines to share the same facilities and smoothen the power production.

Table 1.1 *Notable wind parks.*

Wind park	Roscoe 1,2,3,4	Horns Reef 2	Thanet	London Array 1	Ormonde
Record	Largest worldwide	Largest offshore in Denmark	Largest offshore worldwide	Largest offshore under construction worldwide	Largest offshore under construction using jackets
Status	In operation	In operation	In operation	Under construct.	Under construct.
Type	Onshore	Offshore	Offshore	Offshore	Offshore
Location	Texas	North Sea	North Sea	North Sea	Irish Sea
Country	USA	Denmark	United Kingdom	United Kingdom	United Kingdom
Commission year	$2008-2009$	2009	2010	2013	$2011-2012$
Installation costs [million euro]	700	470	912	2500	570
Area [km^2]	400	35	35	100	9
Owner	E-on	Dong Energy	Vattenfall	Dong Energy, E-on, Masdar	Vattenfall
Park power [MW]	782	209	300	630	150
Park power [local households]	265,000	200,000	240,000	480,000	100,000
Turbine power [MW]	$1-2.3$	2.3	3.0	3.6	5.0
No. of turbines	627	91	100	175	30
Hub height †	$69-80$	68	70	87	100
Shore distance [km]	–	30	11.3	29	10
Water depth [m]	–	$9-17$	$20-25$	25	17
Main support structure	N/A	Monopile	Monopile	Monopile	Jacket, 4 legs
Pile diameter [m]	N/A	3.9	$4-5$	$4.7, 5.7$	1.8
Pile length [m]	N/A	$30-40$	60	≤ 60	40
Pile embedment depth [m]	N/A	$7-17$	$25-30$	≤ 30	≤ 40
Scour protection	N/A	Stones	Stones	None	None

Compiled mainly from the official websites of the wind parks, affiliated consultants, contractors, suppliers or Wikipedia. The hub height † is the distance from the rotor axis to the ground for onshore wind turbines or to the mean water surface for offshore wind turbines. N/A means *not available*.

These advantages make offshore wind parks favorable for populated coastal areas. One only needs to read the newspaper to be reminded of the importance of the two first points. Recently, protests and demonstrations against the construction of wind turbines of offshore dimensions in the forests, moorland and wetlands of Thy in Denmark were held [National Association for Better Environment, 2011]. Not surprisingly, this does not appear credible in the eyes of some for a supposedly *green* industry.

Conversely, two notable and dialectical drawbacks of offshore wind parks compared to onshore ones are:

- *Increased technical challenges*
- *Higher costs*

These are related to key processes such as installation, inspection and maintenance of key components such as cables, transformer stations, support structures and wind turbines out at sea. As indicated by Table 1.1 and stated by Danish Wind Industry Association [2011, p. 2], offshore wind parks are still more expensive than corresponding onshore ones.

It appears to me that the above pros and cons are materialized in several decisions concerning the layout of an offshore wind park. The conflicting interests between reducing *visual impact* and *costs* entail that the offshore wind parks are usually located in shallow waters, say 10–20 m. Furthermore, the sheer volume of the wind turbines in the offshore wind parks imply that minor key changes can breed much influence – for better and for worse. Therefore, the conflicting interests between reducing *economical and technical risks* and *costs* appear to favor a strategy that builds on conventional proven methods and introduces new technology carefully at a smaller scale.

This research is fostered on this background and engages the two drawbacks of offshore wind parks. Of several potential areas that are being researched by others, this research is concerned with a certain aspect of the *support structure* that carries the wind turbine since the support structure accounts for a considerable amount of the total costs.

3.2 km 4.8 km 6.4 km 8 km 16 km 24 km 32 km

Figure 1.1 *Visual impact of a 3.6 MW wind turbine as function of the shore distance.*

Adopted from Garden State Offshore Energy [2011].

1.2 Support structures

A *wind turbine*[1] consists of blades, a rotor, a nacelle (including a possible gearbox and the generator) and finally a tower. The first components are responsible for producing the energy whereas the latter one, the tower, is only used as support for the nacelle and for conveying the cable for electricity and communication. The tower is practically a three-dimensional vertical beam that experiences axial, shearing, bending and torsional forces of dynamic character that must be absorbed by the underlying *support structure*[2].

Now, there are many combinations of structural principle, connectivity, material and production methods. In the following discussion, I will consider three typical candidates of main support structures for offshore wind parks as illustrated in Fig. 1.2:

- *Gravity structure* consisting of a hollow frame of reinforced concrete that is filled with a heavy ballast during installation and that rests on a prepared stone bed.
- Hollow and circular steel *monopile* that is driven into the seabed by a hydraulic hammer until the pile has gained sufficient resistance.
- *Jacket* consisting of a steel truss with legs and braces welded together and the legs grouted onto a group of piles that have been driven into the seabed in advance.

As indicated by the database of Lindoe Offshore Renewables Center [2011] and Table 1.1, the monopile has been and continues to

(a) Gravity structure (b) Monopile (c) Jacket

Figure 1.2 *Examples of support structures.*

Adopted from Rambøll [2011].

be the most common choice with a pile diameter in the range 4-6 m. The gravity foundation is used secondly and can be used on rocky soils in contrast to the two other structures. The jacket has been used extensively in the oil and gas industry but only limited for offshore wind parks. However, these trends may change depending on the fate of the Ormonde park that is being constructed at the moment and will be the largest offshore wind park supported by jackets as shown in Table 1.1.

According to the estimate of Zaaijer et al. [2001], the cost of the support structure is in the order of 1 million euros per unit. This concerns a monopile or tripod and covers expenses related to management, engineering, manufacturing, transportation, installation, maintenance and decommissioning. As we shall see in the following section, about 10 % of these costs can be related to the *scour design* of the support structure that I am focusing on in this research.

1.3 Scour & scour designs

In most cases, the support structure rests on or is near the seabed as for the previously considered main support structures. If the installation of the support structure is sufficiently obtrusive, it may

change the flow of water from its native state. The changed flow may, in turn, change the shape of the local seabed, a process called *scour* that is the central topic of this research. This is illustrated for a monopile in sand in Fig. 1.3.

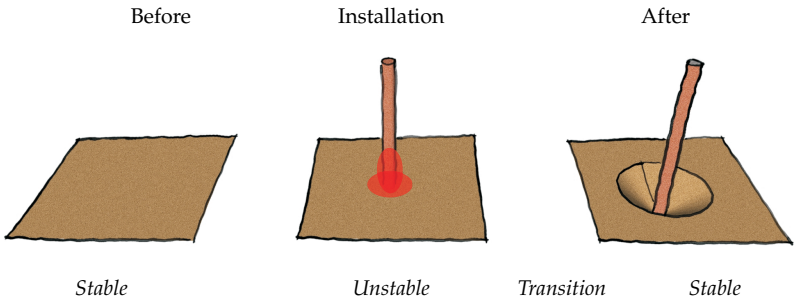

Figure 1.3 *Illustration of scour around an exposed monopile in sand.*

If the dimensions of the bed change were relatively small compared to those of the base of the support structure, scour would be of no practical concern. However, numerous studies show that *the dimensions of the bed change* can *be comparable to those of the base of the support structure* as we shall see later. If so, the changed bed surface can significantly change the performance of the total structure and usually imply a loss of stiffness and strength.

The intensified flow and the resulting scour depths are elaborated later in Chap. 3 for the monopile in sand. For now, it suffices to consider Example 1.1 where I have given an indication of the proportions of the scoured bed for the three support structures. The example indicates that even limited scour will be influential to gravity structure and even maximum local scour can be negligible to jackets. The monopile represents an ambiguous case where the scoured bed can play a role depending on whether it has attained its maximum or only a limited size.

In general, the sensible designer is confronted with three different design approaches to scour:

- *Scour-protected design* that requires scour protection to be installed and assumed no scour to occur.
- *Scour-impairing design* that changes the structural design so as to minimize scour.

Example 1.1 *Dimensions of the scoured bed around exposed support structures.*

Consider the *scour-exposed* gravity, monopile and jacket support structures of typical dimensions in sand. Assume that:

- The scoured bed has developed into a hole around the base of the support structure.
- The hole has the depth S and the radius $R = 1.5\ S$ relative to the outer surface of the structure. This corresponds to a situation where the slope angle is equal to $\phi = \tan^{-1}(S/R) \approx 34\,\mathrm{deg}$.
- The scour depth S is taken to be proportional the base diameter D of the support structure, i.e. $S = c\ D$.
- The coefficient of proportionality c is taken as $c = 0.5$ or $c = 1.5$ for the case of limited or maximum scour, respectively.

This yields the following results:

Main support structure		Gravity structure		Monopile		Jacket	
Scour size		Limited	Maximum	Limited	Maximum	Limited	Maximum
Base diameter D	[m]	10	10	5	5	1.5	1.5
Coefficient c	[m]	0.5	1.5	0.5	1.5	0.5	1.5
Scour depth S	[m]	5	15	2.5	7.5	0.8	2.3
Scour radius R	[m]	7.5	22.5	3.8	11.3	1.1	3.4

- *Scour-exposed design* that allows scour to occur but requires the support structure to be sufficiently resistant to the loss of the supporting seabed.

The scour designs are illustrated in Fig. 1.4 for a monopile in sand and discussed in the following. A supplementary discussion is given by Zaaijer and Templ [2004].

1.3.1 Scour-protected design

To put the scour-protected design into perspective, I want to portray a common type of scour protection, namely *stone protection*. This is shown for the gravity structure and the monopile in Fig. 1.2 and for the monopile also in Fig. 1.4(a).

The stone protection consists of two equally important components. Firstly, a top layer of coarse stones that are too heavy to be

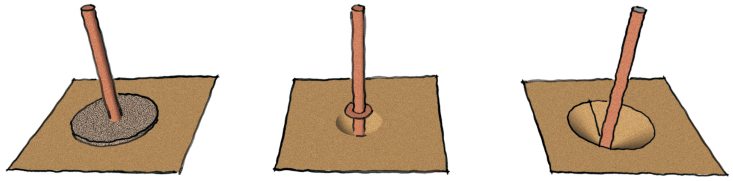

(a) Scour-protected (b) Scour-impairing (c) Scour-exposed

Figure 1.4 *Scour designs.*

dislodged by the changed flow. Secondly, one or more sub layers of successively finer stones that reduce the permeability of the stone protection and thereby hinder the underlying finer bed material from being sucked out. The horizontal extent of the stone protection must match that of the flow change.

To install the stone protection, several steps are required. The stones must be collected and loaded unto a vessel of sufficient size. The vessel must be sailed and positioned near the support structure during favorable weather conditions. Finally, the stones must be dumped in the correct order and at the correct position. These steps are usually carried out *after* the installation of the main support structure and its cables and *before* that of the wind turbine tower and implies that scour can occur in the intermediate period. This is less critical for the performance of the support structure since it is not fully loaded and the time duration is short. However, it may add another considerable step to the installation procedure, namely the step of re-establishing the scoured bed back to a plane configuration by backfilling stones into the scour hole before the stone protection can be built. The volume of additional stones to cover a fully developed scour hole is comparable or even exceeds that of the stone protection, so this step may double the material use.

As I hope to have made clear, the steps involved in using scour protection are laborious. According to the estimates of Halfschepel [2001, 2003] for the 3MW or 6MW offshore wind turbines in the DOWEC project, the use of stone protection costs in the order of 100,000 euro per unit. This covers the use of equipment, personnel, fuel, material and transportation. This amounts to about 10 % of

the unit costs of the support structure according to the estimate of Zaaijer et al. [2001].

1.3.2 Scour-impairing design

In the second approach, the *scour-impairing* design, one introduces artificial structural components near the bed so as to suppress the flow intensity and thus to reduce scouring. This approach relies on an intimate knowledge of the flow features as described later in Chap. 3. Examples of this are a horizontal collar as shown in Fig. 1.4(b) or cables spiraling around the monopile as demonstrated in Dey et al. [2006]. Apparently, a scour-impairing design has only been investigated in the laboratory and has not been employed in the field. The weaknesses of the scour-impairing design is that these approaches add another step to the installation, may become less effective as marine growth appears and can amplify scour if they are not properly installed or the flow configuration differs from anticipated.

1.3.3 Scour-exposed design

In the final approach, the *scour-exposed design*, scour is allowed to occur and the corresponding response of the total structure must be investigated. One can cope with the scour hole by changing the structural performance during design and operation. To do so at the design stage, the dimensioning scour hole must be determined. Depending on how it is determined, I define two flavors of the scour-exposed design:

- *Static* design based on the worst possible scoured bed.
- *Dynamic* design based on the actual scoured bed.

In the *static* design, one considers the worst possible scour configuration. This is usually a scoured bed of comparable dimensions to those of the base of the support structure as previously illustrated. This is simple and safe, but perhaps too conservative in some cases.

The *dynamic* design has the potential of being more economical than both the protected and static exposed design simply because both the scour and load processes are *transient*. Therefore, there can be favorable moments in time when limited scour occurs when the

support structure is intensely loaded. Or alternatively, maximum scour can occur when the support structure is weakly loaded. In fact, this principle is exploited partly in the scour-protected design by allowing scour to occur before the scour protection is installed without taking further measures.

One favorable situation that I investigate in this research is the case when the sea state changes from being dominated by currents to being dominated by waves. The scouring process due to the action of current can be retarded or even reversed by the action of waves. In the latter case, the waves can deposit bed material into the scoured bed so the scour hole becomes smaller, a process that I will refer to as *backfilling*. This phenomenon is quite fortunate because it implies that scour can be limited during storms due to the wind-generated waves.

The costs of the different scour designs are estimated in Example 1.2 for a scour-protected and scour-exposed monopile. In the latter case, the dynamic or static designs are dimensioned with a scour depth $S/D \approx 0.5$. or $S/D \approx 1.5$, respectively. The index values of the example indicate that the costs are comparable. However, the weak trends suggest that the dynamic scour-exposed design is most economical and the static scour-exposed design is most costly.

For the gravity structure, the sheer size of the scoured bed as given in Example 1.1 and its potential of undermining the bed below the base seems to suggest that the scour-protected design is preferable unless the bed is highly erosion-resistant like rock. For the jacket, even a static scour-exposed design appears to be economical and the dynamic design will only amplify this trend.

Weaknesses of the scour-exposed design The scour-exposed design *adds another degree of freedom to the total structure*. This should be understood both in a literal and figurative sense in that the exposed design changes the stiffness of the total structure and complicates matters, respectively. From a perspective of reducing risks, increasing the complexity of an already richly complex structure is not desirable. It may even be prohibited by superior concerns to other structural components.

For example, the total structure experiences considerable dynamic loads at the rotor and blade-passing frequencies of the wind turbine and the peak frequency of the ocean waves. If a scour-exposed monopile is employed as the main support structure, the

Example 1.2 *Influence of scour design on material use and costs.*

This example follows the cost estimate of Oud [2003] that builds on Bakker [2003]. Oud used the reported costs of the scour protection from Halfschepel [2001, 2003] but in this example, I will use a lower cost of 100,000 euros for the scour protection per unit. Furthermore, I have also added my own analysis for the case of limited scour based on the methodology of Oud [2003].

Consider a 3.6 MW or 6.0 MW offshore wind turbine that is to be installed in the Dutch sector of the North Sea in a water depth of $L_2 = 20\ \mathrm{m}$. The main support structure is a scour-protected or exposed monopile.

The pile top is located at a height $L_5 = 10\ \mathrm{m}$ above the mean water level and the pile has the length L_p. The pile is made of steel with a circular and hollow cross section given by the outer diameter D_o and wall thickness t_w. Thus the inner diameter is $D_i = D_o - 2t_w$ and the cross-sectional area is $A = \pi/4\ (D_o^2 - D_i^2)$. The density of the steel is taken as $\rho = 7850\ \mathrm{kg/m^3}$ and thus the pile mass is $m = \rho A L_p$. For the scour-exposed designs, assume the scour depth $L_3 \approx 0.5 D_o$ for limited scour or $L_3 \approx 1.5 D_o$ for maximum scour as in Example 1.1. The embedment depth L_5 is only shown for comparison with Table 1.1 and Example 1.3. It is computed as $L_4 = L_p - L_2 - L_3 - L_5$.

For the scour-exposed designs, assume an additional steel use of 20 ton due to the added length of the J-tube for the cables. Determine the pile dimensions D_o, t_w and L_p for each wind turbine such that pile top experiences identical rotation during the ultimate limit state. Assume that the steel price is 1 euro per kg. Denote a value that has been normalized to that of the corresponding scour-protected case as 'Index'. This leads to the following results:

Wind turbine		3.6 MW			6.0 MW		
Scour design		Protected	Exposed	Exposed	Protected	Exposed	Exposed
Scour hole size		None	Limited	Maximum	None	Limited	Maximum
Hub height L_1	[m]	80	80	80	95	95	95
Water depth L_2	[m]	20	20	20	20	20	20
Scour depth L_3	[m]	0	2.5	7.5	0	3.0	9.3
Embedment depth L_4	[m]	30	31.5	30	35.9	35.2	31.4
Pile outer diameter D_o	[m]	4.6	4.7	4.9	5.8	5.9	6.2
Pile wall thickness t_w	[m]	0.046	0.047	0.049	0.058	0.059	0.062
Pile length L_p	[m]	60.0	64.0	67.5	65.9	68.2	70.7
Pile mass m	[ton]	310	345	396	541	580	664
Index	[–]	100	111	128	100	107	123
Pile material costs	[kilo euros]	310	345	396	541	580	664
Added costs	[kilo euros]	100	20	20	100	20	20
Total considered costs	[kilo euros]	410	365	416	641	600	684
Index	[–]	100	89	101	100	94	107

lack of supporting soil can be interpreted as a lowering of the point of fixation if the total structure is viewed as a cantilever beam as in Example 1.3. The increased beam length will lower the natural frequency of the total structure. To avoid resonance, the changed natural frequency must not overlap with one of the load frequencies. In case of overlap (scenario B in Example 1.3), resonance can be mitigated at the design stage by increasing the tower and monopile stiffness (scenario C) or ensuring that the control system changes the rotor frequency. If such options are not possible, the scour-protected design should be adopted instead.

However, I note that the added degree of freedom and the variation in the apparent point of beam fixation could also be viewed somewhat as a benefit. This is because the dynamic stresses will act on cross-sections at a wider range of elevations instead of being concentrated at a narrower range of elevations near the pile base as in the scour-protected case.

To use the exposed design, one needs to adopt new ways of conveying and protecting the cables that come from the tower. If the cables are freely exposed to the flow, their lifetime is usually severely reduced. At present, the cables are conveyed in J-tubes that run *through* or *on top of* the stone protection and in the latter case, protective mattresses are placed on top of the tubes. In a scour-exposed design, new solutions must be adopted of which a few are discussed in Zaaijer and Templ [2004].

The *dynamic* approach has an additional drawback, namely that it relies on accurate scour forecasts. A quick glance on last month's weather forecast for today can remind us of the humbling fact that *it is easy to make a forecast but difficult to make an accurate one*. In fact, I would go as far to say that the dynamic exposed design is not mature yet for commercial use whether it builds on existing or this research. As I see it, this requires a better quantitative understanding of the processes involving the fluid flow around the support structure and its interaction with the sediment.

* * *

Example 1.3 *Influence of scour design on natural frequency.*

Consider the NREL 5 MW reference wind turbine with three blades as reported by Jonkman et al. [2009] that I will use here except for some aspects of the tower. The hub height is $L_1 = 90\,\mathrm{m}$. The rotor frequency is $f_r \in [6.9; 12.1]\ \mathrm{rpm}$ at operational wind speeds. The mass of the nacelle and the rotor is $m = 350 \cdot 10^3\ \mathrm{kg}$.

Next, assume that the wind turbine is located in shallow waters in the North Sea and that the main support structure is a monopile of typical dimensions with a scour-protected or exposed design. Estimate the peak frequency of the ocean waves as $f_p \approx 0.08$ Hz.

As an approximation, assume that the total structure can be considered as an undamped and massless cantilever beam of length L and with the point-mass m attached to the free end. Assume that the cross section of the beam is homogeneous and has Young's modulus E and second moment of the area I. Use a circular and hollow cross section given by the outer diameter $D_o \approx 6\ \mathrm{m}$ and the wall thickness $t_w \approx 0.025\ \mathrm{m}$ and thus, the second moment of area is $I = (D_o^4 - (D_o - 2t_w)^4)\pi/64 = 2.09\ \mathrm{m}^4$. Then, the frequency of the first bending eigen mode is $f_n = \sqrt{k/m}/2\pi$ where the spring stiffness is $k = 3EI/L^3$. This yields the following results:

Scenario		A	B	C
Scour design		Protected	Exposed	Exposed
Hub height L_1	[m]	90	90	90
Water depth L_2	[m]	15	15	15
Scour depth L_3	[m]	0	12	12
Embedment depth L_4	[m]	20	20	20
Beam length $L \approx \sum_{j=1}^{4} L_j$	[m]	125	137	137
Young's modulus E	[GPa]	210	210	280
Natural frequency f_n	[Hz]	0.22	0.19	0.22
Wave peak frequency f_p	[Hz]	0.08	0.08	0.08
Rotor frequency f_r	[Hz]	$[0.12; 0.20]$	$[0.12; 0.20]$	$[0.12; 0.20]$
Blade-passing frequency $3f_r$	[Hz]	$[0.35; 0.61]$	$[0.35; 0.61]$	$[0.35; 0.61]$
Assessment		Desirable	Undesirable	Desirable

Chapter 2

Aims

Based on the presented context, I outline the broad and specific goals of this research in this chapter.

2.1 Broad goal

The broad goal of this research is:

> *to develop a method that produces accurate scour forecasts for offshore wind parks*.

This is illustrated in Fig. 2.1. On one hand, one is given the long-term temporal curves for the parameters of the *sea state*, such as the water depth, current velocity and significant wave height. On the other hand, the task is to determine the long-term temporal curves for the parameters of the *scour geometry*, such as the scour depth and scour volume. If structural or other parameters were also influential and varying in time, these should also be included as input. The resulting curves for the scour geometry are referred to as the scour forecast. Here, I would like to reiterate my point from Chap. 1, namely that *it is easy to define the scour geometry curves by an equation and draw the solution but difficult to ensure that the underlying definition is accurate*[1].

Accurate scour forecasts are relevant for both a scour-protected and a dynamic scour-exposed design since they provide answers to at least two practical questions:

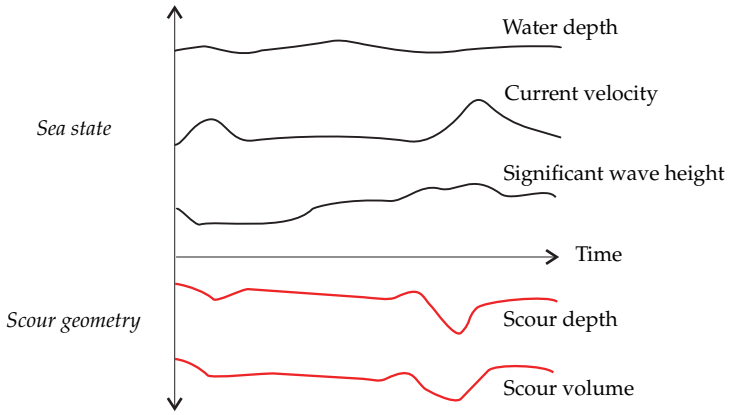

Figure 2.1 *Broad goal = Transient data on sea state ⇒ Transient data on scour geometry.*

- *What is the volume of the scoured bed before the scour protection is installed?* This can be determined directly from the scour forecast. The answer is relevant in the context of a scour-protected design when one plans the vessel capacity or estimates the volume of additional stone material to fill a possible scour hole prior to embarkment.
- *What are the dimensions of a scour-exposed support structure that is resistant to all loads during its lifetime at a particular location?* This can be determined from structural-soil analyses that are coupled together with the scour forecast. The scour geometry is obtained directly or can be estimated from the scour forecast. The properties of the underlying or ambient soil must be estimated. Here, I note that a more refined analysis will not only consider the scour geometry but also the *stiffness* of the seabed as investigated preliminary in Sørensen et al. [2010]. The answer is relevant for determining the feasibility and costs of a dynamic scour-exposed design as an alternative to the other scour designs as done in Example 1.2. Such an assessment is also relevant in another context, namely for bridge piers in rivers that are liable to considerable scour during occasional and sudden floods.

2.2 Specific goal

This research does not claim to attain the broad goal. Instead, it deals with the less ambitious but more tractable *specific goal* of answering the following two dialectical research questions:

- *Which parameters are suited for describing the scour geometry during scouring and backfilling?* This is relevant for establishing the parameters that are going to constitute the scour forecast. In Fig. 2.1, I have presupposed that the scour depth and scour volume are relevant and I motivate this choice in Sec. 4.4.
- *How do the parameters develop in time for a given sea state?* This is relevant for actually making a scour forecast in response to a sea state.

The research questions only concern a circular monopile in uniform sand. This is because the monopile represents both a common and potentially cost-saving case for offshore wind parks. Sand is particularly erosion-prone and is a typical material in the bed surface layers in the North Sea. The research questions are answered in Chaps. 4-5.

* * *

Chapter 3

Review of Scour

A comprehensive review of scour around different support structures is given in e.g. Sumer and Fredsøe [2002] or Whitehouse [1998]. In this chapter, I will recap some central aspects for the monopile, namely the flow features that appear around the monopile and how they are related to the scour process. In the last section, conventional formulas for the depth of the scour hole are reviewed.

3.1 Flow

The seabed is a *deformable* boundary that responds to the intensity of the fluid flow in most practical cases. The phenomenon of scouring arises because the fluid flow can be greatly intensified near a support structure and thus cause a considerable local deformation of the seabed. To understand scour, one must therefore first understand the intensified flow around the monopile. The flow is therefore described in the following sections.

3.1.1 Flow features

Based on Sumer and Fredsøe [2002], Dargahi [1989], Unger and Hager [2007], Zhao and Huhe [2006] and Kirkil et al. [2005, 2008], I have schematized the fluid flow around the monopile for a plane bed. The same flow features can also appear for a *scoured* bed as reported in Kirkil et al. [2008], Yuhi et al. [2000] or Kobayashi [1992] but are naturally influenced by the scoured bed. Some features of

the present flow resembled that of a *free cylinder*, i.e. a cylinder placed transversely in an uniform flow with the considered flow domain being sufficiently far from the lateral boundaries as given in e.g. Sumer and Fredsøe [1997]. Other features are markedly different from the case of the free cylinder due to the present proximity of the seabed. The flow around the pile is shown in its complexity in Fig. 3.1(c). To clarify the origin of this flow picture, I describe the flow with reference to Fig. 3.1(a) in the following outline:

1-2. *Pile and seabed:* The fluid velocity must come to complete rest at the boundaries of the pile and the seabed. This is required by the kinematic and no-slip boundary conditions and assuming that the boundaries are impermeable and at rest. These two assumptions are only approximately satisfied for the seabed since granular materials are permeable and the sediment entrainment that occurs at some locations on the seabed requires that the local fluid velocity is not zero.

3. *Boundary layer inflow:* Since the velocity of the idealized seabed is zero, the imposed flow must develop a boundary layer near the bed.

4. *Down-flow:* The pressure in the fluid in front of the pile is partly dictated by the incoming velocity as suggested by the Bernoulli equation. The incoming streamwise velocity decreases with the depth and will therefore impose a high pressure on the upstream pile surface near the water surface and a lower pressure at lower elevations. The pressure at the lowest elevations increases again due to the stagnation point at the pile toe and the contribution from hydrostatic pressure. The pressure in excess of hydrostatic pressure illustrated in Fig. 3.1(b) in a longitudinal and vertical plane. Following Newtons second law, the fluid particles must travel away from increasing pressure when the deviatoric stresses are relatively small. The illustrated pressure distribution may therefore cause the inflow to separate downwards and cause a down-flow upstream of the pile. The down-flow may further separate near the pile toe.

5. *Horseshoe vortices:* The separated down-flow may bounce upstream (path B in Fig. 3.1(b)). The boundary layer inflow near the bed also experiences an adverse pressure gradient as it approaches the pile and may separate upwards (path D). The

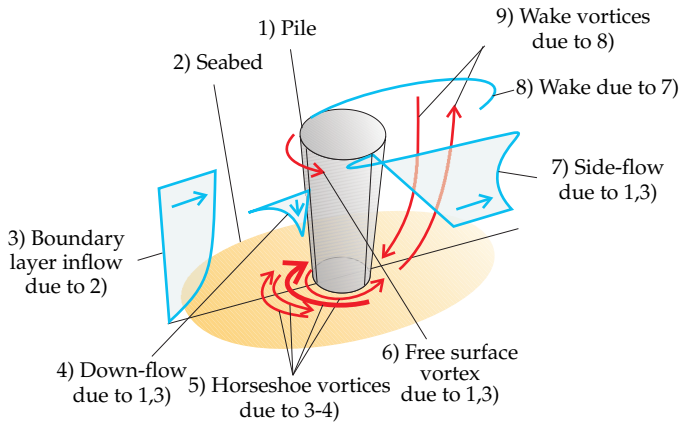

(a) Features of mean flow.

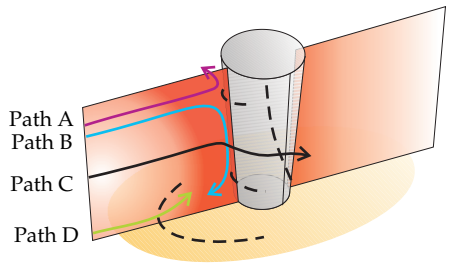

(b) Mean pressure in excess of hydrostatic pressure.

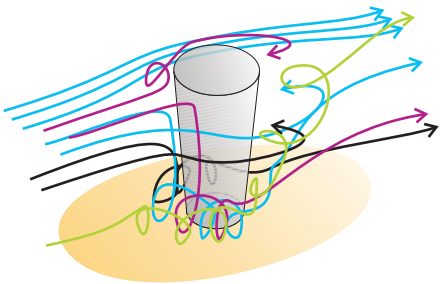

(c) Particle paths of mean flow.

Figure 3.1 *Schematized mean flow around monopile in a plane bed.*

Dashed curves are separation curves. Red arrowed curves are vortex curves.

result of either the up-flow or separated down-flow is the formation of a number of vortices whose vortex curves resemble a horseshoe, referred to here as horseshoe vortices[1]. The arrows of the vortex curves in Fig. 3.1(a) illustrate the direction of rotation using the right-hand-rule.

6. *Free surface vortex:* The inflow near the water surface can separate upwards (path A) when approaching the pile since the pressure at the water surface is relatively smaller. This causes a rise in the free surface in front of the pile and the separated flow may roll around to form a free surface vortex[2].
7. *Side-flow:* The blockage of the pile causes the upstream fluid to eventually travel around the pile shoulders. The side-flow[3] is predominantly two-dimensional far from the bed, resembling the case of the free cylinder. In such a horizontal plane, potential theory suggests that the flow speed doubles near the pile shoulders compared to the incoming flow speed at the same elevation.

8-9. *Wake and wake vortices:* The side-flow begins to decelerate near the pile shoulders and face increasing pressure along the remaining path near the pile perimeter. The increasing pressure may cause the flow to separate (path B). The separated side-flow (detached shear layers) that emanates from each pile shoulder rolls around to form a wake downstream of the pile with one or more pairs of wake vortices. When the horseshoe vortices are present and turbulent, the separation points near the pile shoulder move more behind due to the increase in the turbulence intensity. In this case, the width of the wake decreases with depth and the vortex curves of the wake vortices are oblique such that they are vertical near the water surface and bended towards the pile axis near the bed.

Putting these components together, I have drawn an example of the resulting mean paths of inflowing fluid particles in Fig. 3.1(c) with inspiration from Kirkil et al. [2005, Fig. 3] and Zhao and Huhe [2006].

3.1.2 Variation and suppression

In addition to the above outline, I emphasize that the flow features can vary in several ways. The flow features can be entirely lami-

nar or increasingly turbulent [Domínguez et al., 2006, Baker, 1980]. The horseshoe and wake vortices can vary in number, size, location, shedding behavior and life-span depending on the configuration and the moment in time. For example, several studies demonstrate that the largest of the horseshoe vortices, the primary horseshoe vortex, shifts between two preferred positions during the course of time, see e.g. Kirkil et al. [2008] or Bressan et al. [2011].

This leads to another important point, namely that *the down-flow, horseshoe vortices, free surface vortex, wake or wake vortices can each be partially or fully suppressed in special cases*. In the most suppressed case that in practice only appears to arise for certain wave conditions, the only remaining flow features are the incoming boundary layer and the side-flow. This property of suppression is also the the primary means of demarcating the flow features in the complex flow of Fig. 3.1(c) since the side-flow exists even for the creeping flow around a free cylinder, the wake vortices emerge when the Reynolds number increases for the free cylinder and the horseshoe vortices can appear for the pile. Below, I have briefly recapped the suggested governing parameters of the flow features and the cases when they are suppressed:

- *Down-flow, horseshoe vortices and free surface vortex:* Baker [1980], Melville and Sutherland [1988], Sumer et al. [1992b, 1997], Sumer and Fredsøe [2001] and Roulund et al. [2005] suggest that the horseshoe vortices (and thus also the down-flow) are mainly governed by the normalized boundary layer thickness δ/D, the pile Reynolds number $R_D = U_{cu}D/\nu$, the normalized water depth H/D and for waves, also the Keulegan-Carpenter number $K = U_m T/D$. Here, U_{cu} is the incoming depth-averaged streamwise velocity, D is the pile diameter, ν is the kinematic fluid viscosity, U_m is the amplitude of the near-bed streamwise velocity in a wave flow and T is the wave period. The normalized boundary layer thickness and the Reynolds number govern the adverse pressure gradient. Melville and Sutherland [1988] suggest that the normalized water depth governs the distance between the free surface vortex and the primary horseshoe vortex such that the they are each weakened for shallow depth due to their opposite sign of rotation (see Fig. 3.1(a)). Sumer et al. [1997] reports that the horseshoe vortices are absent for $K < 6$. The effect of increasing K is to allow the horseshoe vortices to acquire their

full strength since the boundary layer thickness is allowed to grow, separation is allowed to occur to form the horseshoe vortices and the flow features are sustained for a longer fraction of each half-period in a wave cycle.

- *Wake and wake vortices:* For the pile or a free cylinder in regular waves, Sumer and Fredsøe [1997] and Sumer et al. [1992b, 1997] suggest that the wake and the shedding regimes are mainly governed by R_D and K. They report that the wake first appears at the Keulegan-Carpenter number $K \approx 1 - 2$ and shedding of wake vortices begins at $K \approx 6 - 7$. Here, the effect of increasing K is again to allow the wake features to develop to their full measure as governed by R_D. For example, K limits the possible number of shedding events that can occur during each half-period of the wave cycle.

3.2 Stress amplification

The fluid stresses near the bed are responsible for entraining the sediment. The intensified flow illustrated in Fig. 3.1 amplifies the local magnitude of these stresses compared to those of the far-field and therefore results in scouring near the pile. Below, I briefly illustrate how this occurs and the interaction is discussed further in Chap. 5.

3.2.1 Process

The process can be illustrated by considering the upstream vortices near a pile in a scoured bed. The vortices are manifested in the streamlines of Fig. 3.2 or the vortex curves of Fig. 3.1(a). Similar arguments can be given for the wake vortices.

The vortex cores contain rapidly-swirling fluid particles. As shown in Fig. 3.2, the streamlines below the vortices contract considerably and cause amplified velocity gradients. These are in turn associated with an amplification of the bed shear stress as given readily by the flow field and the employed constitutive relation for the Newtonian fluid. The erosive action of the deviatoric stresses is illustrated for the sediment particle A in Fig. 3.2. Furthermore, the high velocities in the vortex cores are associated with a reduction of the pressure compared to the surroundings as suggested by the Bernoulli equation. If the gradients of the deviatoric stresses are

relatively small, this pressure gradient can suck fluid and sediment particles into the cores and perhaps further along the trajectory of the vortex curves (shown in Fig. 3.1(a)) like a vacuum cleaner. The erosive action of the pressure gradient is illustrated for sediment particle B.

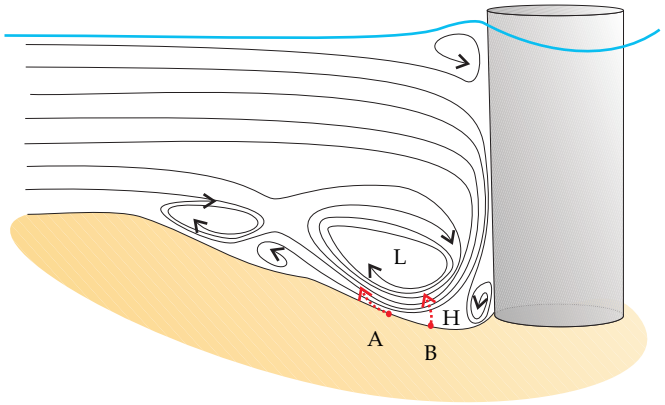

Figure 3.2 *Streamlines of the mean two-dimensional flow upstream the pile for a scoured bed.*

Streamlines inspired from Unger and Hager [2007] and Kirkil et al. [2008]. L and H indicate zones of low and high pressure, respectively.

Once the sediment is entrained from the bed, it travels near the bed or is convected away along the mean flow paths of the flow features and follow vortices if they are shed off. The entrained sediment settle in more peaceful regions downstream in the near-field. For frictional soils, the local erosion can cause the local slope angles to increase until the repose angle at which local sliding failure occurs. Sliding usually causes multiple holes to collapse into one larger one at some point during the scouring process.

Observations suggest that the bed evolution is retarded, if not fully stopped, once the initial seabed has developed into a scoured bed comparable to the pile dimension. This scoured bed is referred to as the *equilibrium bed* [Melville and Chiew, 1999, Barbhuiya and Dey, 2004]. However, as detailed in the following section, the flow is still quite intense for the equilibrium bed. This paradox can only be explained by requiring that the sediment becomes more erosion-resistant in the case of an equilibrium bed compared to a plane bed such that the gained resistance retards or suppresses further scouring. The latter case is conveyed in the term *equilibrium*. Returning to

Fig. 3.2, it is apparent that most of the horseshoe vortices, especially the primary horseshoe vortex, are rotating clockwise and will therefore shear the particles more or less *upslope*. In this case, the stabilizing effects of gravity in terms of increased static resistance and/or possibility of nearly continuous local sliding failure can explain the gain in erosion-resistance for friction soils against the erosive action of deviatoric stresses. If the gained erosion-resistance is observed to fully or nearly balance the effect of scouring during clear-water conditions, it is expected that a weak inflow of sediment caused by a live-bed condition will backfill the scour hole and cause gentler slopes and lower scour depths until the erosive resistance and flow intensity are again balanced. This is consistent with the findings of Melville and Sutherland [1988] where maximum scour is obtained in the limit between clear-water and live-bed conditions for uniform sediment.

3.2.2 Stress amplification factors

As illustrated and discussed in Sec. 3.1, the amplification of fluid stresses depends on the configuration and requires a detailed experimental or numerical flow study. Based on a few notable model-scale studies, I give a rough assessment below of the amplification factors caused by the flow features so as to identify which flow features are primarily responsible for scouring. I mainly consider the magnitude of the mean bed shear stress τ' compared to the far-field magnitude, i.e. $M \equiv \tau'_{\max}/\tau'_{\text{ref}}$, since this is most commonly reported.

- *Side-flow:* The least amount of flow amplification for any quantity under consideration is expected in the most suppressed case where the only flow features are the boundary layer inflow and the side-flow. The corresponding amplification below the side-flow around a pile in a plane bed can be estimated crudely by assuming that the inflow speed doubles at the pile shoulder as suggested by potential theory and computing the amplified bed shear stress using the Colebrook-White formula as given in Ref. 1. This provides $2.75 \leq M \leq 4$ and is consistent with the wave experiments of Sumer et al. [1997, Figs. 22-23] reporting $M \approx 3-4$ at the pile shoulder or slightly upstream of the pile shoulder for $K \leq 20$. These ranges are slightly higher than the earlier results $M \approx 2-3$

at the pile shoulder that were reported for comparable wave conditions by Sumer et al. [1992b, Fig. 6]. For a scoured bed, the incoming flow may decelerate as it enters the scour hole as in a diffuser flow and the amplification in the side-flow is expected to be considerably weakened.

- *Horseshoe vortices:* Sumer et al. [1997], Roulund et al. [2005] and Kirkil et al. [2008, 2009] together suggest that the *mean* amplification of the bed shear stress below either of the horseshoe vortices in a plane or equilibrium bed can be as large as $M \approx 11$. Even higher amplification has been reported for laminar flows [Yuhi et al., 2000, Umeda et al., 2003]. Kirkil et al. [2008] further demonstrates that for the two bed points shown in Fig. 3.3(a) in terms of the friction velocity, the standard deviation of the *instantaneous* amplification of the bed shear stress is about $1.25M$ and it can be much higher in other instants. For a plane bed, the location of the zone of maximum M is reported approximately midways between the pile toe and pile shoulder (Roulund et al. [2005], Kirkil et al. [2009, p. 899]). For an equilibrium bed, one of the maximum zones is found in front of the pile toe below the primary horseshoe vortex as shown in Figs. 3.2–3.3. Kirkil et al. [2008] also reports an amplification of an order of magnitude in the pressure correlation and the turbulent kinetic energy inside the horseshoe vortices. Several studies report that the intermediate bed between the plane and equilibrium bed experiences the most most intense horseshoe vortices. This has been reported in terms of the mean bed shear stress in Yuhi et al. [2000] or vorticity of the mean flow and turbulent kinetic energy in Bressan et al. [2011].
- *Wake vortices:* There appears to be no amplification in the *mean* bed shear stress inside the wake according to the time-averaged unsteady results of Roulund et al. [2005, Fig. 26b] for a plane bed or according to Kirkil et al. [2008, 2009] for an equilibrium bed, i.e. $M \approx 1$ in this case. However, the latter studies reveal again that the amplification in the instantaneous bed shear stress is comparable to that of the mean flow as illustrated in Fig. 3.3. Furthermore, the amplification in the pressure correlation and turbulent kinetic energy is comparable to, if not higher than, those produced by the horseshoe vortices (see Kirkil et al. [2008, Figs. 6,13] and Kirkil et al.

[2009, Figs. 9,13]).

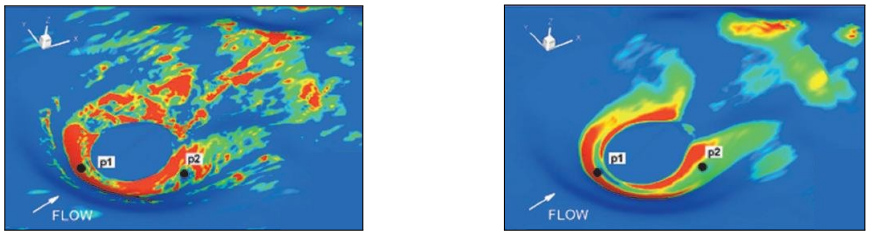

(a) Instantaneous (b) Mean

Figure 3.3 *Magnitude of friction velocity U'_f for a pile in an equilibrium bed subjected to current.*

Red denotes increased magnitude. Adopted from Kirkil et al. [2008].

3.2.3 Scouring agents

Based on the preceding considerations and assuming that the model-scale flow studies can be taken as somewhat representative for field-scale, I suggest the following rough classifications concerning the flow features that are responsible for the scouring process:

- *Current:* For most practical cases involving current, horseshoe vortices exist and amplify the mean and instantaneous bed shear stress persistently. Furthermore, the erosion of the slope base near the pile and subsequent local sliding can further accelerate the scouring process. Conversely, the action of the wake vortices appears to be more intermittent and local sliding is expected to be less pronounced in the wake due to the adverse action of the outflow. This is also consistent with the observed gentler slopes downstream than upstream. Therefore, horseshoe vortices appear to be the primary scouring agent in this case.
- *Short-stroke waves:* For waves with extremely low Keulegan-Carpenter number, taking $K < 6$ from Sec. 3.1.2, vortex shedding is suppressed and horseshoe vortices are not present. Therefore, the only possible scouring agent appears to be the side-flow.

- *Other cases:* For all other cases, the horseshoe vortices, wake vortices and side-flow may be equally responsible for scouring. The side-flow and wake vortices are retained because they exhibit amplification in the mean and instantaneous bed shear stress, respectively. Sumer et al. [1993] and Sumer and Fredsøe [2001] suggests that shedding of wake vortices is the primary scouring agent in this case but do not reason why the action of the horseshoe vortices is to be considered relatively inferior to the wake vortices in these cases.

3.3 Scour development

In the following, the focus is turned towards predictive formulas for clear-water and live-bed scour based mainly on model-scale laboratory tests. The focus is partly on the temporal development of the scoured bed since this is at the heart of scour forecasting. Furthermore, offshore wind parks are typically exposed to combinations of current or waves and will typically be in live-bed conditions as demonstrated in Example 3.1. Therefore, the focus is also on the *live-bed* frameworks. The considered frameworks characterize the scoured bed by its depth S and the suitability of this is discussed in Chap. 4. Besides laboratory tests, numerical scour studies are at present less reliable but some are referenced in Chap. 5. Temporal field-scale studies in wave-exposed locations are scarce as reviewed in Whitehouse et al. [2011].

3.3.1 Clear-water scouring

Several suggestions have been set forth concerning the scour depth development during clear-water conditions of which some are referenced in Barbhuiya and Dey [2004, Sec. 5.8]. Two notable frameworks are the analytical formula of Melville and Chiew [1999] or the ordinary differential equation of Dey and Barbhuiya [2005]. The former formula builds on the equilibrium scour depth formula of Melville and Sutherland [1988] that is based on a large base of clear-water or live-bed studies mainly from the laboratory and some from the field. The estimated equilibrium scour depth represents a maximum (enveloped) value and is found to be $S/D = 2.4$ for a monopile that can be favorably reduced for shallow water depth, coarse or graded sediment or live-bed conditions. Other formulas

Example 3.1 *Typical sea states for offshore wind parks.*

This example demonstrates the typical conditions for offshore wind parks. The monopile has diameter $D = 4$ m and is placed in water depth of 10 m in the North Sea. The sea state consists of combinations of current and waves where the wave height and wave period are taken from the Danish Wave Energy Program [Energistyrelsen, 1999, p. 19]. The near-bed wave velocity U_m is computed from Stokes' fifth order theory with nil current and taken under the wave crest at the bed. The bed shear stress τ'_{r_∞} and near-bed current velocity $U_{cu,D/2}$ are computed as in Ref. 1, using either the Colebrook-White formula for current alone or the boundary layer models of Fredsøe [1984] for the remaining cases. In the latter, τ'_{r_∞} represents the maximum magnitude obtained during a wave cycle. The bed is assumed to be plane. The equilibrium scour depths are computed from Table 3.1 and the index values have been normalized to that of the current-alone case.

The following parameters have been used for the fluid, sediment and flow. The fluid has the mass density $\rho_f = 1000$ kg/m^3 and kinematic viscosity $\nu = 10^{-6}$ m^2/s. The sediment has the median grain size $d = 0.20$ mm, relative grain-fluid density $s = 2.65$, the critical Shields number $\zeta_c = 0.05$ and takes the gravitational acceleration as $g = 9.81$ N/kg. The flows use the Karman constant $\kappa = 0.4$ and Nikuradese roughness $k = 2.5d$. The Keulegan-Carpenter number associated with the wave velocity is computed as $K_w = U_m T/D$, the Reynolds number as $R = (U_m + U_{cu})D/\nu$ and the undisturbed Shields number as $\zeta'_{r_\infty} = \tau'_{r_\infty}/(\rho_f g d \cdot (s-1))$. The latter is used to determine whether the erosion regime is clear-water ($\zeta'_{r_\infty} < \zeta_c$) or live-bed ($\zeta'_{r_\infty} > \zeta_c$). The analysis leads to the following results:

Scenario		A	B	C	D	E	F	G
Current		Medium	None	Medium	None	Medium	None	Medium
Waves		None	Small		Medium		Large	
Water depth	[m]	10	10	10	10	10	10	10
Depth-averaged current velocity U_{cu}	[m/s]	1	0	1	0	1	0	1
Near-bed current velocity $U_{cu,D/2}$	[m/s]	0.96	–	0.94	–	0.91	–	0.90
Wave height	[m]	–	1	1	3	3	5	5
Wave period T	[s]	–	5.6	5.6	8.4	8.4	11.2	11.2
Near-bed wave velocity U_m	[m/s]	–	0.28	0.28	1.26	1.26	2.3	2.3
Bed shear stress τ'_{r_∞}	[Pa]	1.1	0.4	2.2	4.5	7.8	12.5	17.1
Shields number ζ'_{r_∞}	[–]	0.34	0.12	0.68	1.4	2.4	3.9	5.3
Reynolds number R	[–]	$4 \cdot 10^6$	$1.1 \cdot 10^6$	$5.1 \cdot 10^6$	$5.2 \cdot 10^6$	$9.2 \cdot 10^6$	$9.2 \cdot 10^6$	$1.3 \cdot 10^7$
KC number K_w	[–]	–	0.4	0.4	2.7	2.7	6.4	6.4
Current-wave ratio c_{cuw}	[–]	1	0	0.8	0	0.4	0	0.3
Erosion regime	[–]	Live-bed	Live-bed	Live-bed	Live-bed	Live-bed	Live-bed	Live-bed
Normalized equil. scour depth S_∞/D	[–]	1.3	≈ 0	0.1	≈ 0	0.2	≈ 0	0.3
Index for S_∞/D	[–]	100	0	9	0	18	1	25

for the equilibrium scour depth are reviewed in Jensen et al. [2006, Rep. 2].

3.3.2 Live-bed scouring

It appears that there is only one framework for considering the temporal development during live-bed and wave conditions, namely the work of Sumer, Fredsøe and co-workers. This work is also recognized in the guidance of the offshore standard for offshore wind parks [Det Norske Veritas, 2004, App. J]. Sumer et al. [1992b,a, 1993, 2007] and Dey et al. [2006] examined scouring around a monopile in an initially plane bed subjected to steady current *or* regular waves. They quantified both the temporal and equilibrium scour depth and suggested the following formula for the scour depth development:

$$S = S_\infty \cdot \left(1 - e^{-t/t_S}\right) \tag{3.1}$$

where S is the actual scour depth at time t, S_∞ is the equilibrium scour depth and t_S is a time scale for the scour depth development. The time scale was suggested to scale as:

$$t_S = \frac{t_S^* D^2}{\sqrt{g d^3 \cdot (s-1)}} \tag{3.2}$$

where $s = \rho_d/\rho_f$ is the relative grain-water density, ρ_d is the density of the solid grains, ρ_f is the density of the fluid, g is the gravitational acceleration, d is a characteristic grain size and t_S^* is a normalized time scale.

In the study of Sumer and Fredsøe [2001], scouring in irregular waves with or without superimposed current was examined and the results for the equilibrium scour depth were quantified in Sumer and Fredsøe [2002, p. 198]. The initially plane bed was scoured by waves alone, then scoured further by superimposing a weak current and scoured even further by successively increasing the current speed[4]. Between each flow change, the equilibrium bed was allowed to develop and the equilibrium scour depth was measured. The time scale for these experiments was not investigated.

Assessment Based on these campaigns on live-bed scouring, it was found that the largest equilibrium scour depth was obtained during current $S_\infty/D \approx 1.3 \pm 0.7$, the smallest depth during short-stroke waves $K \to 0 \Rightarrow S_\infty/D \to 0$ and intermediate scour depth

for intermediate cases. These trends are incorporated in the formulas for the equilibrium depth in Table 3.1 and have been exemplified in Example 3.1. The results for S_∞ during current are in the same order of magnitude as the field-scale review in Whitehouse et al. [2011] or Melville and Sutherland [1988] but appear to be an approximation compared to the latter since there are no reducing factors during current. The observation of the role of the Keulegan-Carpenter number, i.e. K or K_w, in diminishing the scour depth is consistent with its role in suppressing the action of horseshoe vortices and wake vortices as discussed in Sec. 3.1.2. Here, K_w is associated with the contribution from the waves in a combined wave-current case. Example 3.1 demonstrates the possibility of limited scour depth below $S/D = 0.3$ in typical wave conditions for offshore wind parks, provided that the formulas are valid at field-scale.

Concerning the time scale formula (3.2), the authors did not present the rationale behind it in these studies but limited argumentation appears in gross terms in Whitehouse [1998] and Sumer and Fredsøe [2002, p. 70]. One one hand, the formula (3.2) is also supported by the model-scale live-bed experiments of Ballio et al. [2010]. One the other hand, other authors employ a different scaling and e.g. Melville and Chiew [1999] normalize the time scale as $t_S = t_S^* D/U_{cu}$ for clear-water scouring.

Concerning the formula for the *normalized* time scale as given in Table 3.1, the selection of the considered parameters has been reasoned and discussed in Sumer et al. [1992a, 1993]. The undisturbed Shields number $\zeta'_{r_\infty} = \tau'_{r_\infty}/(\rho_f g d \cdot (s-1))$ is considered to be one of the governing parameters. The two formulas for current alone and waves alone do not match in the limit $K \to \infty$ and do not quantify the influence of the Reynolds number so they are in principle only valid for the considered experimental conditions. As suggested by Example 3.1, it is particularly the change in the Reynolds number that is prominent when going from model to field-scale.

Overall, some notable weaknesses of this framework for scouring appears to be that the experiments are 'only' model-scale and have not been validated by other research groups. Furthermore, the validity of the framework has not been demonstrated for backfilling. This is investigated in Chap. 4 based partly on the work of Thomsen [2006]. Aside from this, backfilling has also been treated recently in Sørensen et al. [2010] and Petersen and Locatelli [2010].

Table 3.1 *Model parameters.*

Load condition	Equilibrium scour depth	Normalized time scale
Current alone	$S_{\infty,cu}/D = 1.3 \pm 0.7$	$t_S^* = \frac{\zeta'^{-2.2}_{r_\infty}\delta/D}{2000}$
Waves alone	$S_{\infty,w} = S_{\infty,cu} \cdot \left(1 - e^{-0.03(K-6)}\right)$	$t_S^* = \frac{\zeta'^{-3}_{r_\infty} K^3}{10^6}$
Current and waves	$S_{\infty,cuw} = S_{\infty,cu} \cdot \left(1 - e^{-A\cdot(K_w - B)}\right)$, $A = 0.03 + 0.75 r_{cuw}^{2.6}$, $B = 6e^{-4.7 r_{cuw}}$, $r_{cuw} = \frac{U_{cu,D/2}}{(U_{cu,D/2} + U_{m0})}$, $K_w = \frac{U_{m0} T_p}{D}$	–

* * *

Chapter 4

Legacy I: Framework for Scour Geometry

In this chapter, I present my first legacy, namely *a framework for scour geometry* with scour forecasting in mind. The chapter builds partly on the concepts introduced in Ref. 1, developed further in Ref. 3 and discussed briefly in Ref. 2. However, this chapter is in itself a new contribution in the sense that it collects these findings and reviews them in a unified, systematical and critical way that has not appeared before.

My answer to the first research question, i.e.:

> *Which parameters are suited for describing the scour geometry during scouring and backfilling?*

mainly considers three aspects, namely how the parameters are obtained, defined and related to the physical process. In the first three sections, I therefore review bed measuring techniques, definitions of possible scour geometry parameters and the development of the scour geometry as indicated by the present model-scale experiments. In Sec. 4.4, I give my verdict and recommend the combined use of the scour depth S and the scour volume V. I also introduce a scour shape factor ψ to couple S and V together.

My answer to the second research question, i.e.:

> *How do the parameters develop in time for a given sea state?*

is given Sec. 4.5 for some configurations. Based on the results from the experiments, I derive and review several equations for describ-

ing the parameter development. I also investigate the tempting alternative of generalizing the equation (3.1) of Sumer, Fredsøe and co-workers. I arrive at recommending the use of a particular set of equations for the scour volume and the scour shape factor such that the scour depth is implicitly determined from these.

4.1 Bed measuring techniques

The scour geometry parameters are confined and influence by the way they have been obtained from measurements, so in this section, I will review some common bed measuring techniques.

If we assume that the interface between the water and soil is sufficiently sharp, we can refer meaningfully to it as the *seabed* and express it as the continuous bed elevation h from a reference level as function of the xy-plane. To obtain the bed elevation at one or more points, we rely on different measuring techniques. Below, I have collected some techniques mainly for laboratory use in connection with scour, grouped them in four categories and illustrated some in Figs. 4.1–4.3:

- *Bathymetry techniques:* The bed elevation at a *multitude of points covering the considered domain* is obtained from a movable submerged laser (this research), rotating laser inside transparent pile [Link, 2006a], movable optical sensor [Ballio and Radice, 2003], sonar [Whitehouse et al., 2011], stereo vision [Baglio et al., 2001] or the manual use of a ruler.
- *Probe techniques:* The bed elevation at *one or few points in the considered domain* is obtained from ruler, gravity-based rod [Sørensen et al., 2010], environmental-sensitive rods partially buried in the seabed employing principles of piezoelectricity or time-domain reflectometry [Lueker et al., 2010]) or fixed versions of the bathymetry techniques.
- *Scour domain imagery:* The bed is viewed by human eye, photograph or video from one direction and the *dimension-tagged image* is processed.
- *Pile base imagery:* The bed elevation at one or more points *at the base of the pile* is obtained by processing a dimension-tagged image. This category can be decomposed into two further categories defined by the cases when the viewer is:

- *External/Internal* to the pile as employed in Roulund et al. [2005] or Chiew [1984], respectively.
- *Fixed/Rotating* as employed in [Petersen and Locatelli, 2010] or [Raaijmakers and Rudolph, 2008], respectively.

The techniques have their pros and cons in terms of simplicity, obtrusion to flow or bed, data accuracy, data sampling frequency and data spatial domain. Most laboratory experiments employ *pile base imagery* that is usually straightforward to set-up, operate and process, is non-obtrusive to the flow and bed, and provides millimeter-accurate instantaneous data of the bed elevation at the pile base. In contrast, the *bathymetry technique* in terms of a movable submerged laser employed in the present experiments require specialized software to control and process, must be operated during a pause in the flow generation to reduce flow obtrusion and consumes some time to obtain the data of the bed elevation over a wider domain. Scour domain imagery can be useful for establishing whether the far-field bed is in a clear-water or live-bed state but appears to be too crude for estimating the bed configuration. For field use, the attributes of costs, durability, power delivery and data acquisition become important too.

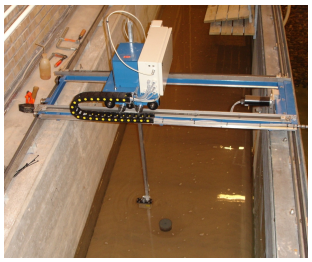

(a) A submerged laser mounted on a movable device along the walls of the flume.

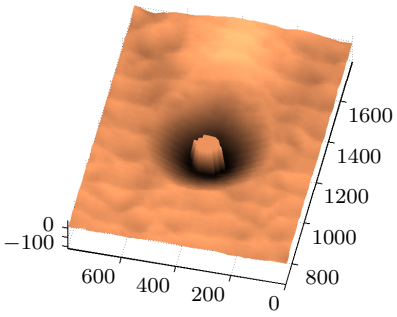

(b) Output: Bed elevation on a spatial grid. The bottom-piece of the pile is also profiled here.

Figure 4.1 *Example of bathymetry technique.*

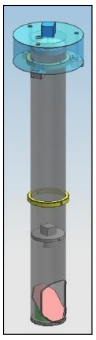

(a) Rotating tube with mirror.

(b) Pile with installed tube.

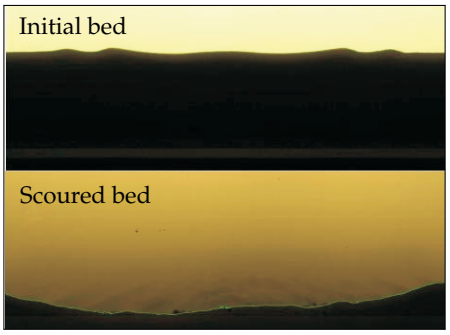

(c) Output: Panoramic image of the bed elevation along the pile base.

Figure 4.2 *Example of internal pile base imagery.*

Adopted from Raaijmakers and Rudolph [2008].

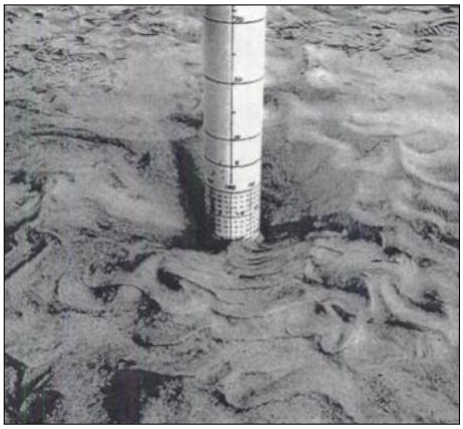

Figure 4.3 *Example of external pile base imagery.*

Adopted from Roulund et al. [2005].

4.2 Scour geometry parameters

If the bed changes near the pile are appreciable compared to surrounding bed and resemble a coherent void around the pile, we can meaningfully characterize the scoured bed as a *scour hole*. A typical example of such a case is shown in Fig. 4.4 and has been obtained from the presently employed bathymetry technique.

As indicated by the preceding conditional clause, the concept of a scour hole is not always meaningful. For example, the initial scouring from a plane bed is observed to begin at the lateral points of the pile so it would be more precise to speak of *two* holes at this stage. Or the process of backfilling can ultimately diffuse the border between the scour hole and the surrounding bed so the distinction can no longer be maintained. The common denominator of these cases is that bed changes nearest the pile are small relative to the pile and will therefore be of less practical concern in the context of scour forecasting. To use the concept of a scour hole for the entire scour process, we will therefore accept that the concept is illusive for the 'smallest holes' but is meaningful for larger scour holes. To be consistent, this implies that *we accept a poor accuracy of the scour forecast on the 'smallest holes' but maintain the requirement of high accuracy for the larger holes*. This implication will be invoked frequently in assessing the parameters and their development.

We want to parametrize the geometry of the scour hole so we can assess, compare and model the parameters. Using the lowest level of detail, I will review some *fundamental parameters* at an arbitrary moment in time. I consider the scour length L, scour breadth B, scour depth S, scour area A and scour volume V. I have defined the parameters conceptually in Fig. 4.4 and more detailed in the following sub sections.

4.2.1 Scour depth

The scour depth S is used by virtually all researchers but with different definitions. I have collected five notable definitions of the scour depth in a given instance in time. The definitions are visualized in Fig. 4.5 and outlined below:

- *Global maximum:* Maximum depth (i.e. minimum bed elevation) anywhere in the bed domain as used by Faraci et al. [2000] or Baglio et al. [2001].

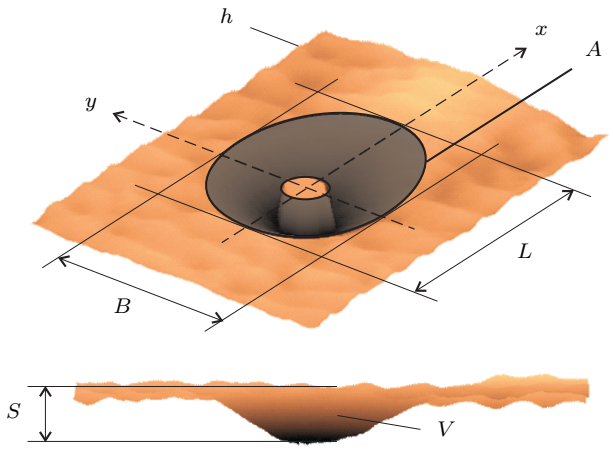

Figure 4.4 *Scour hole and its fundamental parameters.*

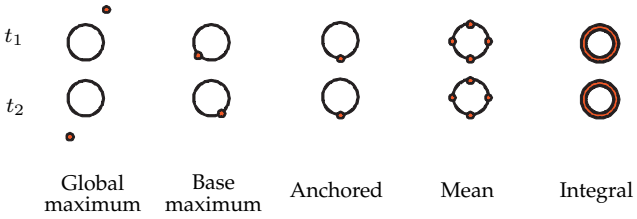

Figure 4.5 *Various definitions of the scour depth S.*

- *Base maximum:* Maximum depth anywhere at the *pile base* as used by Link and Zanke [2004], Link [2006a].
- *Anchored:* Depth at a fixed point at the pile base, e.g. at the upstream or downstream point of the pile as used by Faraci et al. [2000], Baglio et al. [2001] or Roulund et al. [2005].
- *Mean:* Mean depth of a few fixed points at the pile base as used by Sumer et al. [1992a,b, 1993], Sumer and Fredsøe [2001].
- *Integral:* Mean depth of 'all' points along the pile base as I introduced in Ref. 1. The integral depth is defined more formally in Ref. 3 as:

$$S(t) = -\frac{1}{2\pi}\int_{-\pi}^{\pi} h(r = r_{\min}, \theta, t)\, d\theta \tag{4.1}$$

Above, $r \geq 0$ is the radius from the pile axis and $\theta \in [-\pi; \pi]$ is the counterclockwise angle relative to the streamwise direction x. The pile base is thus defined as the closed curve fulfilling $r = r_{\min}$. For example, a circular pile with outer diameter D yields a circular boundary with $r_{\min} = D/2$. The negative sign in (4.1) accounts for the opposite definition of positive directions of h and S.

I have assessed these definitions with respect to reliability, measurability and physical significance as summarized in Table 4.1. The *global maximum* depth excels in detecting the maximum depth that may govern the geometry of the scour hole during sliding as we shall see later. However, it requires a bathymetry technique, has low reliability since it is based on a single point and will not necessarily detect local bed changes if these were also physically important. The *anchored* depth is probably the easiest one to obtain experimentally, but also has low reliability and will not detect a local or global maximum that is located elsewhere. With equal weights on the three considered attributes, I assess that either the *mean* or *integral* definitions are the best choices for scour forecasting.

Table 4.1 *Assessment of definitions for scour depth.*

Definition	Global maximum	Base maximum	Anchored	Mean	Integral
Reliability	Low	Low	Low	Medium	High
Measurability	Low	Medium	High	High	Medium
Importance	Medium	Medium	Low	Medium	Medium
Popularity	Low	High	High	High	Low

4.2.2 Remaining parameters

The remaining fundamental parameters are used less commonly and only supplementary compared to the scour depth. The scour area A is reported in the line of work of Faraci et al. [2000] or Baglio et al. [2001]. The scour volume V is used in the line of work of Link

and Zanke [2004], Link [2006a,b] and by myself. The scour length L or breadth B are used occasionally, e.g. Link and Zanke [2004].

To use the scour length L, scour breath B or scour area A, either scour domain imagery or a bathymetry technique can be employed. In contrast, the scour volume V requires the bathymetry technique. For all of these parameters, the outer boundary of the scour hole must be estimated. This could be done from contour plots or vertical cross-sections of the bed elevation as shown later in Figs. 4.7–4.8. In general, the outer boundary can be defined as the closed curve fulfilling $r = r_{\max}$ and the *scour domain* can then be defined as the span of domain enclosed by $r = r_{\min}$ and $r = r_{\max}$. In Ref. 1, I assumed that $r_{\max}$ could be described as an ellipse but in Ref. 3, I adopted a slightly different definition describing it as a circular-elliptic curve. Once the outer boundary has been determined, the parameters can be computed as follows with reference to Fig. 4.4:

$$L(t) = r_{\max}(\theta = 0, t) + r_{\max}(\theta = \pi, t) \tag{4.2}$$

$$B(t) = r_{\max}(\theta = -\pi/2, t) + r_{\max}(\theta = \pi/2, t) \tag{4.3}$$

$$A(t) = \int_{\theta=-\pi}^{\theta=\pi} \int_{r=r_{\min}}^{r=r_{\max}(\theta,t)} r \; dr \; d\theta \tag{4.4}$$

$$V(t) = -\int_{\theta=-\pi}^{\theta=\pi} \int_{r=r_{\min}}^{r=r_{\max}(\theta,t)} h(r, \theta, t) \; r \; dr \; d\theta \tag{4.5}$$

The negative sign in the definition of the scour volume (4.5) again accounts for the different sign conventions.

I want to make two important practical comments here. First, *the presence of surrounding bed forms can complicate the task of determining the outer boundary*. This is apparent from Fig. 4.7 as presented later. Consequently, the derived parameter are prone to subjective interpretation. For L, B and A, this curse will persist as bed forms appear in most live-bed cases and the uncertainty is governed by the dimensions of the bed forms. In typical model-scale experiments, this means that the uncertainty of L or B is about two orders of magnitude higher than that of the scour depth, i.e. being decimeter-accurate rather than millimeter-accurate. For the scour volume V, the influence of the location of the outer boundary diminishes as the scour hole grows since the bed elevation closer to the pile base will contribute more to the scour volume. If only the outer boundary

covers the main bulk of the scour hole and the scour hole is large enough, the exact location of the outer boundary is of less importance for the value of the scour volume. As argued in the section introduction, the errors of the scour volume for the smaller holes are acceptable.

Secondly, the bed elevation obtained from any bathymetry technique is inherently discrete since it has only been measured over a discrete spatial grid. Consequently, discretization errors are introduced when evaluating the integrals for A and V in Eqs. (4.4)–(4.5) (and for S in (4.1)). To reduce the discretization error within an acceptable margin, the resolution of the spatial bed grid must be sufficiently fine.

4.3 Scour geometry development

The scour hole develops over time and the previous parameters must be able to capture these changes. In this section, I will review some typical features of the scour geometry development based on the present model-scale experiments. I begin by recapping the experiments, then outline the key observations and finally suggest the expected underlying physical process.

4.3.1 Experimental overview

In 2006, Jess McCann Thomsen conducted a series of interesting scour tests in the laboratory flumes of Aalborg University and Ghent University as part of his MSc study at Aalborg University [Thomsen, 2006]. When I started my PhD two years later, I was fortunate to be able to get in touch with him and get access to the data and have conservations with him about the test set-up and procedure. Since I found some aspects of his analysis and conclusions incomplete, I subjected the data to my own analysis and concepts and presented a revised analysis in Ref. 1.

The experiments concerned a model-scale monopile with pile diameter $D = 0.10$ m that was subjected to current and/or irregular waves. At several instances in time during the experiments, the flow generation was temporarily paused and the upper-piece of the pile temporarily dismantled to allow a movable laser device to measure the bed surface in the vicinity of the pile as shown in Fig. 4.1. Five test series were conducted of which most were in the

live-bed regime. In series A, the flow was alternated between current or irregular waves such that both scouring or subsequent backfilling occurred as shown in Fig. 4.6. In series B, tidal current was investigated. In the remaining series, the profiled spatial grid did not cover the entire scour hole so the scour volume could not been obtained for these.

The present experiments are unique in treating the temporal and spatial development of backfilling around a monopile. However, it also became apparent along the way that *the present experiments are impaired in several respects.* This is due to the following items: Lack of documentation for the estimation of the sediment and fluid properties, poor documentation for the experimental procedure and set-up, poor documentation of the elevation for measuring the current speed, abrupt initiation/termination the pump during scouring tests, loss of some data series for waves or current and poor documentation of the relation between photos or camera recordings on one hand and the test runs on the other hand. These uncertainties are not confidence-inspiring and can only be redeemed by repeating the experiments in the future.

Following the conventions introduced in Ref. 3, I use the term *scour* to refer broadly to bed changes around the support structure and this encompasses the sub case of *scouring* when the scour volume is growing and the sub case of *backfilling* when the scour volume is shrinking. I implicitly assume that the porosity of the bed and the density of the bed material remain constant, so the apparent bed change does not stem from changes in these but can only arise from a change of the sediment volume or mass in the scour domain.

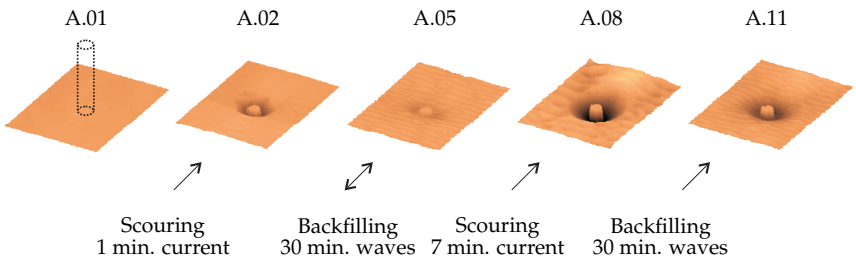

Figure 4.6 *Scour process.*

4.3.2 Observations

The development of the scour geometry is shown in Fig. 4.7 and Fig. 4.8. The measurements are taken from the consecutive runs A.05–11 that begin from a backfilled bed and experience a total of 7 minutes of live-bed current scouring and 30 minutes of live-bed wave backfilling A.05. The shown time is relative to that of the initial bed, i.e. run A.05. Based on these and the remaining test runs of series A, I have schematized the development in Fig. 4.8(c)–(d) and outlined the observations in the following sub sections.

Live-bed current scouring The bed slope in the upstream scour domain – both in upstream and lateral directions – becomes and remains approximately linear once it has reached the repose angle that is $\phi_r = 32\,\mathrm{deg}$ for these tests. In contrast, the bed slope in the downstream scour domain is typically curved and less steep. The fact that the downstream slope is curved makes it less meaningful to characterize it by a single slope angle. The shape of the outer boundary of the scour hole resembles a droplet, being semi-circular upstream and prolonged downstream. Irregular ripples emerge in the near-field but not inside the scour hole. A deposition bank develops downstream of the scour hole.

Live-bed wave backfilling Laterally, there is a considerable deposition at the pile base that results in less steep lateral slopes. The scour breadth appears to be approximately constant with respect to time for most of the runs but grows for the smallest scour hole (A.01-A.05). Longitudinally, the slopes retain their shape as time goes for the large scour holes (A.14-17 and A.20-23) but the slope angles decrease for the smaller scour holes (A.01-A.05 and A.08-A.11). The latter effect can be seen in Fig. 4.8(b). The scour length as obtained from contour curves with levels $h = 0$ or $h \approx -0.02\,\mathrm{m}$, depicted clearest in Fig. 4.7(b-c), appears to be constant or decrease with respect to time, respectively. If the latter contour is adopted, this means that the outer boundary goes from being droplet-like to being approximately circular. Regular ripples emerge across the bed and even inside the scour hole. The shoreward bank is diminished.

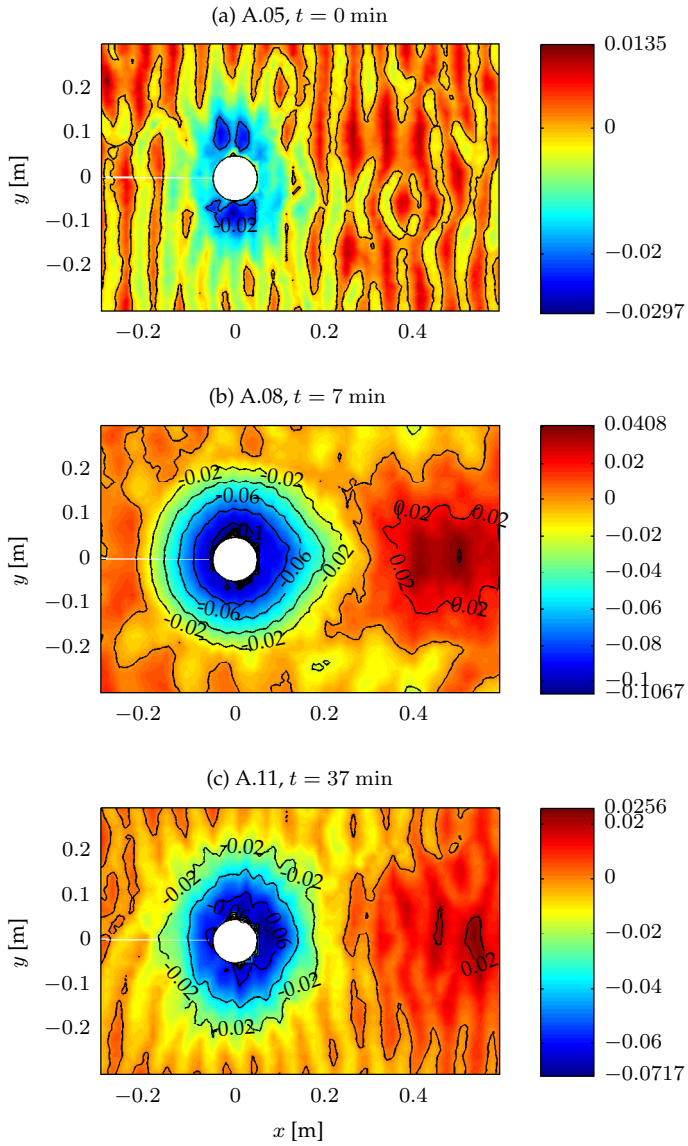

Figure 4.7 *Measured bed elevation and contours.*

All spatial dimensions in meter.

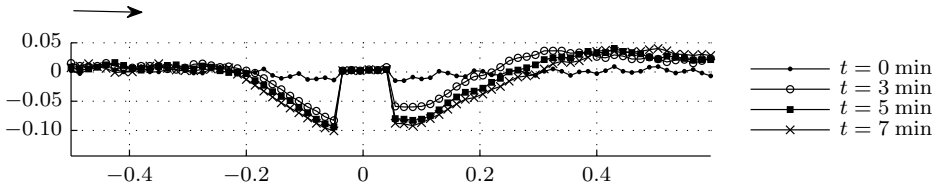

(a) Live-bed current scouring, measured. Test runs A.05-A.08, all spatial dimensions in meter.

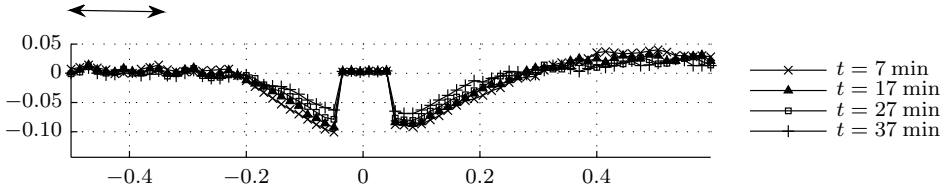

(b) Live-bed wave backfilling, measured. Test runs A.08-A.11, all spatial dimension in meter.

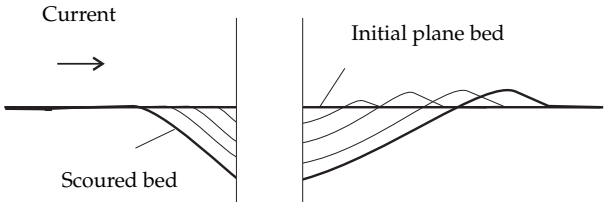

(c) Scouring, schematized.

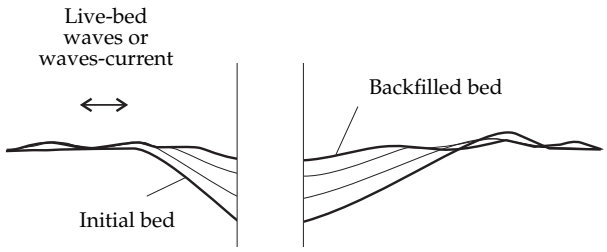

(d) Backfilling, schematized.

Figure 4.8 *Bed elevation at longitudinal vertical sections.*

4.3.3 Hypothesized physical process

Finally, I want to suggest the underlying physical process that may be responsible for these particular observations. The flow studies referenced here are relevant for the present experimental conditions..

Live-bed current scouring For the fluid process, I have mainly consulted the numerical studies of Roulund et al. [2005] and Zhao and Huhe [2006] for scoured configurations comparable to the present experiments. The physical process is schematized in Fig. 4.9 where the grains are colored to visualize their journey during the scouring process. The sequence of the hypothesized process consists of the following four consecutive events:

1. *Sediment erosion* occurs where the flow intensity is amplified compared to the far-field. The grains upstream of the pile (shown in red) are entrained into the cores of the horseshoe vortices whereas the grains downstream of the pile (green) are entrained into the trails of the horseshoe vortices or the cores of the wake vortices (Fig. 4.9b). The observation of a steep upstream slope and gentler downstream slope suggests that, on average, the intensity of the flow and erosion is higher upstream than downstream for a scoured bed. This is consistent with the similar distribution of the time-averaged bed shear stress for a scoured bed as reported in Roulund et al. [2005, Sec. 6.2] or Zhao and Huhe [2006, Fig. 9-10].
2. Subsequent *sliding failure* occurs mainly upstream of the pile (orange) since the slope base is presumingly eroded and the slope angle is already close to the repose angle (Fig. 4.9c). This is strongly supported by the observed semi-circular shape of the outer boundary in the upstream region of the scour hole and the well-defined relation between the scour radius and the scour depth (see Sec. 4.2.2 of Ref. 3).
3. *Sediment transport* occurs along the trajectories of the fluid particles (Fig. 4.9c).
4. *Sediment deposition* occurs where the amplification of the flow intensity diminishes. The observed emergence of a bank immediately downstream of the scour hole implies that some of the inflowing and eroded grains are deposited here and thus

the flow intensity must, on average, be diminished here. By exclusion, the remaining grains must be perpetually held in suspension near the scour hole, deposit in the scour hole, deposit downstream of the bank or travel into the live-bed far-field (Fig. 4.9d).

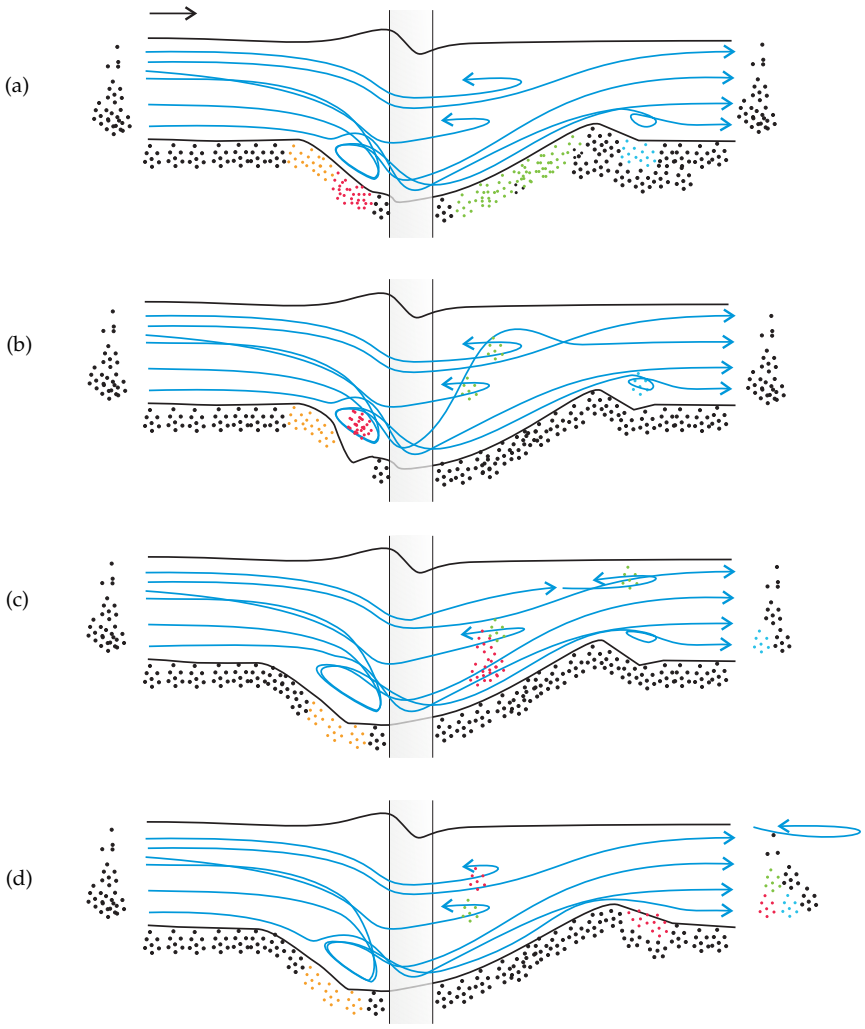

Figure 4.9 *Live-bed scouring process.*

Live-bed wave backfilling For the fluid process in waves, I have exploited the insights from the fluid studies of the previous section and also consulted some additional fluid studies. The flow under waves and the associated boundary layers without the pile is described in e.g. Fredsøe and Deigaard [1992]. The wave flow around a pile in a plane bed has been investigated by Sumer et al. [1997] and is supported by Faraci et al. [2000]. For the flow around a pile in a scoured bed, I have consulted the somewhat comparable study of Kobayashi [1992] treating non-linear regular waves and secondly Umeda et al. [2008] treating a laminar oscillatory flow.

A reasonable requirement for backfilling to occur appears to be that *the far-field is in a live-bed state* as observed in the wave runs of series A, D and E (see e.g. Fig. 7 of Ref. 1). Based on this assumption, I envision that the over-all physical process goes as follows.

The grains within a radius of the stroke a from the outer boundary of the scour domain are liable to convect and backfill into the scour hole. The stroke can be estimated as $a = U_{m0}/\omega$ where U_{m0} is the significant streamwise fluid velocity above the boundary layer in the far-field, $\omega = 2\pi/T_p$ is the circular frequency and T_p is the wave peak period, giving $a \approx 5$ cm in the wave runs of series A. Consequently, the departure region is eroded to some degree but is also backfilled partially by the grains that were eroded $2a$ from the outer boundary. The over-all effect of such a chain of erosion and deposition appears to be that *the sediment is distributed evenly across the seabed* when neglecting the presence of bed forms. Consequently, after a sufficient number of wave cycles, the near-field is eroded and the scour hole is backfilled compared to the initial condition. This is consistent with the observation in Fig. 4.8(b).

The expected physical process is further schematized in Fig. 4.10. The irregular waves of the experiment are for clarity drawn as regular waves. The phase is taken as $\xi = \omega t - kx$ from linear wave theory where $k = 2\pi/L_w$ is the wave number, L_w is the wave length. The wave crest is above the pile axis when $\xi = 2\pi j$ where j is an integer. The figure focuses on the journey of the grains immediately seaward of the outer boundary (shown in red) and, although not shown, similar processes are expected to occur elsewhere near the outer boundary of the scour hole. The sequence of expected events is outline below:

1. *Sediment erosion* occurs slightly shoreward of the position of the wave crest or trough where the flow intensity is largest.

The bed one stroke a seaward of the outer boundary of the scour hole is eroded (red). Due to the considered configuration of the dimensions of the scour hole and the waves, erosion occurs in the scour hole shortly after (green) as shown in Fig. 4.10b-c. At the end of the half-cycle, erosion in the scour hole occurs seaward of the pile (blue, Fig. 4.10e).

2. *Sediment transport* occurs along the orbital particle trajectories of the wave flow and the trajectories of the horseshoe or wake vortices, if they emerge. This convection can occur in serial such that grains are supplied by the orbital flow and then conveyed further by the vortices. The grains eroded from the near-field convect shorewards into the scour hole and are dispersed around the pile. The grains eroded from the scour hole are convected seawards and are dispersed above the scour hole (Fig. 4.10c-d). As discussed in Sec. 5.2 of Ref. 3, the Keulegan-Carpenter number is $K \approx 3$ for the present wave runs and wake vortices are expected to be present and perhaps also shedding. The possibility of shedding at this lower value for K may be possible due to the irregular nature of the waves in contrast to the regular waves considered in Sumer et al. [1992b]. In the study of Kobayashi [1992] for a somewhat comparable configuration, upstream horseshoe vortices are absent and this suggests the absence or at least a limited life-span of the upstream horseshoe vortices in the wave runs of series A, presumingly due to the low Keulegan-Carpenter number.
3. *Sediment deposition* occurs during flow reversal and death of the vortices. Some of the convected grains fall into the scour hole to be deposited later. By exclusion, the remaining grains are maintained in suspension by wake vortices that are washed around the pile or deposit into the near-field (Fig. 4.10e). The observation of deposition laterally to the pile suggests that, on average, the flow intensity is weaker here than at both the shoreward and seaward points of the pile.

I have not added a bullet point for sliding since it appears to adopt a more anonymous role in the present backfilling tests compared to the case of scouring. One one hand, the eroding action of the vortices at the base of the slopes could still occur as suggested by Fig. 4.10(b),(f). On the other hand, the present observations in

terms of decreasing scour depth along all base points, gentler lateral slopes, constant scour breadth, constant or decreasing scour length indicate that *sliding occurs more locally and does not dictate the over-all dimensions of the scour hole*. This is presumingly due to the absence or reduced life-span of the horseshoe vortices as discussed in the second bullet above.

4.4 Parameter selection

Drawing mainly on the preceding findings, I here give my recommendations for the suitable parameters for scour forecasting.

4.4.1 Scour depth and scour volume

I recommend the combined use of the scour depth S and the scour volume V for scour forecasting. The reasons for retaining the scour depth are given below:

- The data for the scour depth can be obtained from a variety of bed measuring techniques, and most notably from pile base imagery that is simple and unobtrusive. In contrast, bathymetry techniques are required for obtaining V and recommended for obtaining L, B, A. The latter three parameters can alternatively be estimated roughly from scour domain imagery at a lower accuracy.
- The scour depth can be defined unambiguously as discussed in Sec. 4.2.1 and is insensitive to the definition of the outer boundary of the scour hole.
- During scouring, erosion of the base of the upstream slope and subsequent sliding plays an important role in characterizing the development of the scour geometry. This erosion can be directly related to the scour depth S of a suitable definition and the scour depth in turn partly dictates the development of L, B, A and V.
- The scour depth is already used extensively for scouring. A continued use can therefore build on existing scour research.

I introduce the scour volume V due to the following reasons:

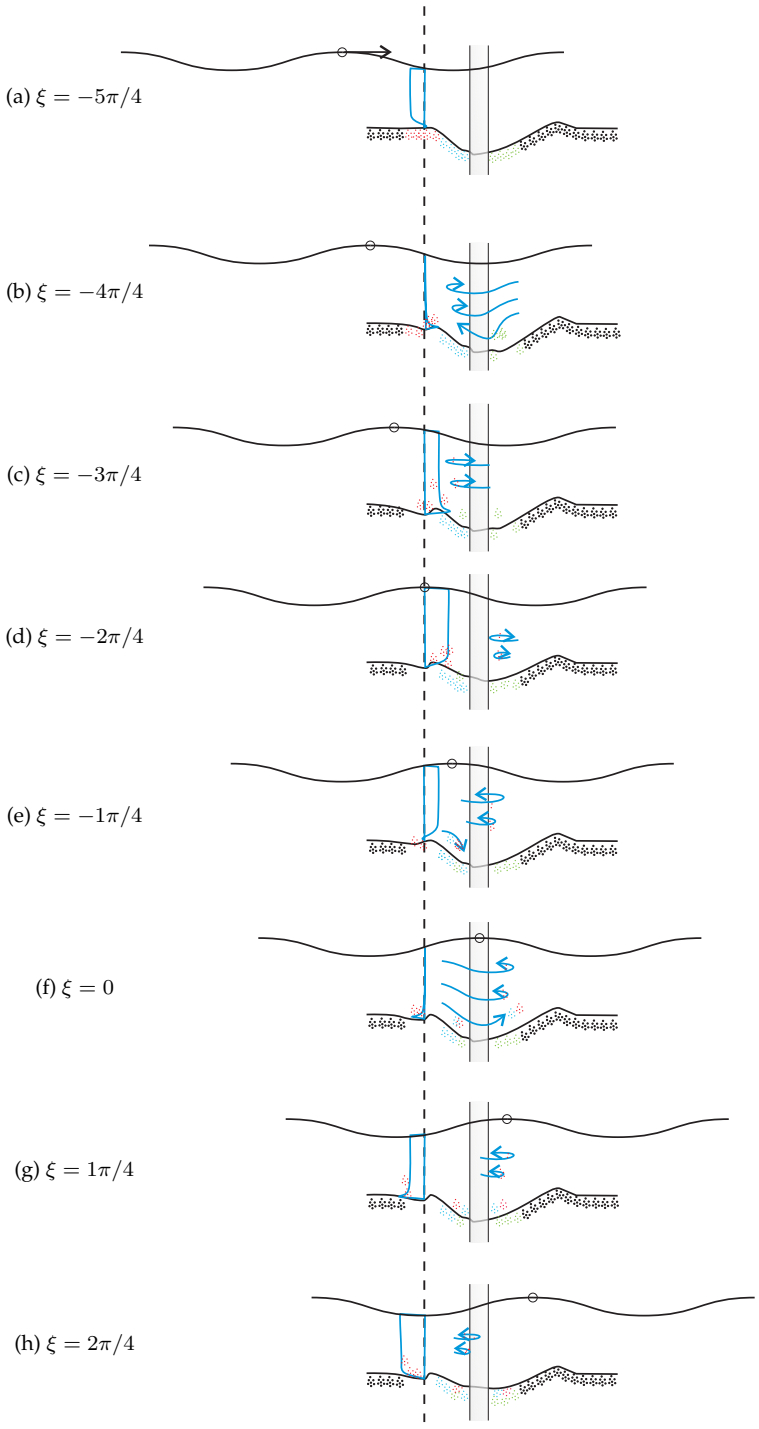

Figure 4.10 *Live-bed wave backfilling process.*

- During backfilling, sliding can occur more locally such that it may no longer uniquely characterize the development of the scour geometry. For example, two scour holes stemming from scouring or backfilling can have the same scour depth but have markedly different shapes. To characterize the scour hole during both scouring and backfilling, the scour depth must therefore be supplemented by another fundamental parameter.
- L, B or A are sensitive to the exact location of the outer boundary of the scour hole that can be difficult to assert during typical live-bed and model-scale conditions. In contrast, the scour volume becomes insensitive to the exact location of the outer boundary as the hole grows.
- For scour-protected designs, the scour volume is the wanted parameter from the scour forecast for determining the volume of backfilled stones.
- As shown in Sec. 5.3 of Ref. 4, the rate of the scour volume can be related to the volume rates of the fluxes of the bed load and suspended load. Thus, the use of the scour volume can build on existing research from sediment transport.
- As we shall see in Sec. 4.5, the rate of the scour volume rate can be described by a development equation that fits well with the present experiments.

Together, the scour depth and the scour volume appear to offer the best description of the bed surface during scouring and backfilling as I will demonstrate later in Sec. 4.5.5. However, the introduction of the scour volume comes at a price: It requires the use of a bathymetry technique. Those insisting on a continued use of solely the scour depth can exploit the depth-based similarity approach that is introduced later in Sec. 4.5.4 at the loss of some accuracy.

4.4.2 Scour shape factor

To couple the scour volume and scour depth, I introduced a new parameter in Ref. 1, the so-called *scour shape factor* ψ. The scour shape factor is defined through the following implicit relation:

$$V \equiv \psi S^3 \tag{4.6}$$

Another length scale could also have been adopted instead of S in (4.6), but the assessment in Sec. 4.4.1 suggests that the most sensible choice is the scour depth in favor of any other length scale.

If the scour hole is scaled uniformly in all dimensions, then by definition, the original and scaled holes are *geometrically similar*. I investigate the implications of geometrical similarity in Example 4.1 and Example 4.2. It follows from (4.13) in the latter example that for a scour hole that develops in a geometrically similar fashion, the scour shape factor is constant with respect to time, i.e.:

$$\text{Geometrical similarity} \Rightarrow \frac{d\psi}{dt} = 0 \tag{4.7}$$

It is now apparent that the use of the scour shape factor has two advantages. First, it offers a intuitive indication of the shape of the scour hole. A plane bed will have $\psi \to \infty$, developed current-scoured holes reach a minimum $\psi \approx 3 - 8$ and wave-backfilled holes experience intermediate values as shown later in Sec. 4.5.3. Secondly, the development of the scour hole during scouring can be modeled *approximately* by taking the scour shape factor to be constant with respect to time as introduced later in the similarity approaches of Sec. 4.5.4.

Before I proceed, a word of caution concerning the hypothesis of geometrical similitude is appropriate. Initially, I overlooked the fact that *scour holes can never develop in a perfectly geometrically similar way*. This fact can be easily proven by considering the case when the fundamental length parameters of the *scour hole* are scaled uniformly but the *pile diameter* remains unchanged. Thus, *all* dimensions have not been stretched uniformly and the scour holes of such a case can only be *approximately geometrically similar*. The approximation would be negligible if the fundamental length parameters were overwhelmingly larger than the pile diameter. However, since the scour dimensions are typically smaller or comparable to the pile, the error never disappears. Therefore, the assumption of geometrical similarity can at best only be approximately valid. If the scour shape factor does become constant during scouring, as it appears to do in these experiments, this only implies that the *shape has changed* to compensate for the constant scour shape factor.

Example 4.1 *Geometrical similitude and proof of volume condition.*

Consider a body of arbitrary form in the three-dimensional Euclidean space. The body has the initial volume V_0. Partition the body into n cubes, each with the side length l_0 and volume $p_0 = l_0^3$. The partition has the initial volume $P_0 = np_0$.

Consider a subsequent deformation where the body and the partition is scaled uniformly in all dimensions such that all distances are multiplied with a constant scale factor r. The initial and scaled pairs of the bodies or the partitions are understood to be *geometrically similar*. For example, a scale factor $r = 2$ implies a doubling of all dimensions as illustrated below.

The uniform scaling implies that each *scaled* cube has the side length $l_1 = rl_0$ and the scaled volume $p_1 = l_1^3 = r^3 l_0^3 = r^3 p_0$. Consequently, the volume of the scaled partition is $P_1 = np_1 = r^3 P_0$.

If we repeat the analysis in the limit of an infinitesimally fine partition resolution, $n \to \infty$ and $P_0 \to V_0$, we obtain the same result. Thus, we infer the general conclusion that *the volume of a body of any form in Euclidean space is proportional to the cube of the scale factor as the body undergoes uniform scaling in all dimensions*, i.e.:

$$\text{Geometrical similarity} \Rightarrow V_1 = r^3 V_0 \tag{4.8}$$

The volume condition (4.8) is commonly exploited for converting volumetric units. For example, to convert between liters and cubicmeters, one exploits $1 \text{ liter} = (0.1 \text{ m})^3 = 0.001 \text{ m}^3$, irrespective of the geometry of the volume.

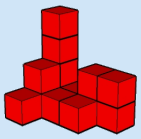

(a) Original partition, $n = 14$ cubes.

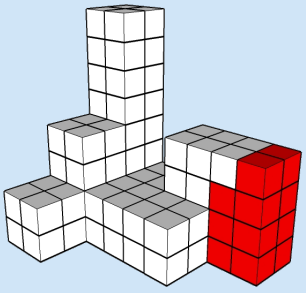

(b) Scaled partition with doubled dimensions, $n = 14$ scaled cubes or $2^3 n = 112$ original-sized cubes.

Example 4.2 *Geometrical similitude and the shape factor.*

Consider a body of arbitrary form in the three-dimensional Euclidean space. The body has the initial volume V_0. Define an arbitrary length scale λ, say the distance between two distinct points of the body, and rewrite the volume in terms of that length scale as:

$$V_0 = \psi_{\lambda_0} \lambda_0^3 \tag{4.9}$$

The coefficient of proportionality ψ_{λ_0} is here denoted the *shape factor* and relates the chosen length scale to the volume. Subject the body to a subsequent deformation and express the new volume in terms of the deformed length scale:

$$V_1 = \psi_{\lambda_1} \lambda_1^3 \tag{4.10}$$

If the deformation consisted of an uniform scaling of all dimensions, the volume condition (4.8) in Example 4.1 implies:

$$V_1 = r^3 V_0, \quad r = \lambda_1 / \lambda_0 \tag{4.11}$$

Exploiting (4.9) and (4.11) yields:

$$V_1 = \psi_{\lambda_0} \lambda_1^3 \tag{4.12}$$

By comparing (4.12) with (4.10), it is seen that the shape factors of both cases are identical, i.e. $\psi_{\lambda_0} = \psi_{\lambda_1}$. This leads to the general conclusion:

$$\text{Geometrical similarity} \Rightarrow \frac{d\psi_\lambda}{dt} = 0 \tag{4.13}$$

The arrow in (4.7) only goes from left to right since a constant shape factor does not *guarantee* a geometrical similar transformation. For example, the dimensions of a ball and a pyramid can be chosen so as to yield the same shape factor but they are clearly not geometrically similar.

4.5 Parameter development

In the preceding sections, I focused on selecting suitable parameters. In this section, I will consider the second research question and focus on *selecting suitable development equations* that can describe the temporal development of the parameters. In the following, I introduce the development equations from Ref. 1 and Ref. 3 and in the last section, Sec. 4.5.5, I assess their performance.

4.5.1 Development of scour depth

Intuitively, it would be natural to attempt to generalize (3.1) so as to cover also scouring from backfilled beds and backfilling in general. As reported in Whitehouse [1998, p. 19] or introduced in Ref. 1, this results in the following linear ordinary differential equation (ODE) for the scour depth:

$$\frac{dS}{dt} = \frac{S_\infty - S}{t_S}, \quad t > 0 \tag{4.14a}$$

which has the solution:

$$S = S_\infty + (S_0 - S_\infty)\, e^{-t/t_S} \tag{4.14b}$$

where S_0 is the scour depth of the initial bed. I note that (3.1) and (4.14b) are identical when $S_0 = 0$ and both equations share the same ODE (4.14a). The behavior of the scour depth equation is discussed in connection with the equation for the scour volume in the following.

4.5.2 Development of scour volume

Based on the experiments in series A, I found that the scour volume V during both scouring and backfilling approximately satisfies the following ODE:

$$\frac{dV}{dt} = \frac{V_\infty - V}{t_V}, \quad t > 0 \tag{4.15a}$$

which has the solution:

$$V = V_\infty + (V_0 - V_\infty)\, e^{-t/t_V} \tag{4.15b}$$

Here, V_0, V_∞ and $t_V > 0$ are fitting parameters that are constant with respect to time and interpreted as the scour volume of the initial bed, the scour volume of the equilibrium backfilled bed and a characteristic time for the scour volume development, respectively. V_∞ and t_V are presumingly dependent on the sea state.

The behavior of the development equations for the scour depth (4.14) or the scour volume (4.15) can be deduced from their ODE formulations and is illustrated in Fig. 4.11. The equation dictates that the scour volume rate dV/dt, i.e. the tangential slope in the plot V vs. t, decreases in magnitude with increasing time or decreasing absolute difference between the initial and equilibrium scour volume. In other words, the scour volume will always seek its equilibrium value and do this more vigorously the further from equilibrium.

I want to make three notes here. First, the equation does not capture the cycles about the equilibrium live-bed state as documented by Chiew [1984] or Ballio et al. [2010], presumingly due to migration of bed forms. Secondly, a careful inspection of the parameter development in the tidal runs in series B suggests that there can be *local* states of equilibrium. This can be treated in (4.15) by changing the values of the equilibrium value V_∞ and possibly also the time scale t_V. Thirdly, the time scale t_V can be related to the amount of volume that has been scoured or backfilled. Denoting the volume at time $t = t_V$ as V_{t_V} and using (4.15b), we obtain $V_{t_V}/V_\infty = 0.63$ for scouring from a plane bed $(V_0 = 0)$ and $V_{t_V}/V_0 = 0.37$ for backfilling to a plane bed $(V_\infty = 0)$. The first result has also been recognized by earlier researchers. These ratios suggest that roughly half of the potential scouring or backfilling has occurred in terms of the scour volume when the time reaches the time scale t_V. However, the analysis also underscores that the mentioned results are only approximately valid in a general case $(V_\infty \neq 0, V_0 \neq 0)$ and also rely on the validity of the equation.

4.5.3 Development of scour shape factor

The present experiments revealed that the development of the scour shape factor depended on whether the scour regime was scouring or backfilling. The combined ODE for both scouring and backfilling is given below where the chain rule has been exploited:

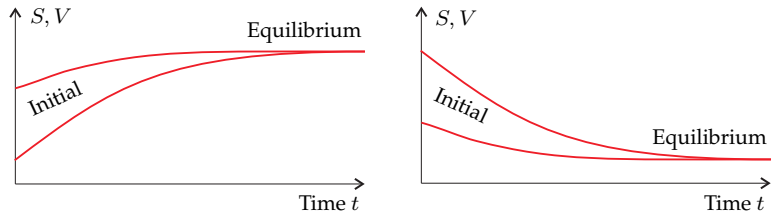

(a) Scouring (b) Backfilling

Figure 4.11 *Behavior of development equations for scour depth or scour volume.*

$$\frac{d\psi}{dt} = \begin{cases} \left.\dfrac{d\psi}{dt}\right._{*}, & \text{Scouring} \\ \left.\dfrac{d\psi}{d(V/D^3)}\right._{**} \cdot \dfrac{dV}{dt}\dfrac{1}{D^3}, & \text{Backfilling} \end{cases} \tag{4.16}$$

Scouring For scouring, it was difficult to achieve a generally valid fit but a similar differential equation as in (4.15) can be used:

$$\left.\frac{d\psi}{dt}\right._{*} = \frac{\psi_\infty - \psi}{t_\psi}, \quad t > 0 \tag{4.17a}$$

which has the solution:

$$\psi_* = \psi_\infty + (\psi_0 - \psi_\infty)\, e^{-t/t_\psi} \tag{4.17b}$$

where ψ_0, ψ_∞ and $t_\psi > 0$ are fitting parameters that are constant with respect to time and are interpreted as the scour shape factor of the initial bed, the scour shape factor of the equilibrium scoured bed and a characteristic time for the scour shape factor development, respectively.

Fig. 4.12(a) demonstrates that the scour shape factor tends to decay towards a minimum value during scouring, being about $\psi_\infty \approx 7 - 8$ in the present tests. A comparison can be made to the line of work of Link [2006b] by digitizing and pairing his figures of the scour volume and scour depth in Link and Zanke [2004, Fig. 3,5] and Link [2006b, p.52-53]. He apparently based the scour depth on a base maximum definition and the scour volume on the contour $h = 0$. The corresponding scour shape factor also exhibits a decay towards a minimum but the minima are lower than the present ones, namely $\psi_\infty \approx 6$ for clear-water scouring and $\psi_\infty \approx 3$

for live-bed scouring, apparently independently of changes in the water depth.

Backfilling For backfilling, the following differential equation was approximately satisfied:

$$\frac{d\psi}{d(V/D^3)}_{**} = -c_1 \cdot \left(\frac{V}{D^3}\right)^{-c_2} \tag{4.18a}$$

which has the solution:

$$\psi_{**} = \psi_0 + \frac{c_1}{c_2 - 1} \cdot \left(\left(\frac{V}{D^3}\right)^{1-c_2} - \left(\frac{V_0}{D^3}\right)^{1-c_2}\right), \quad c_2 \neq 1 \tag{4.18b}$$

where ψ_0, c_1 and c_2 are dimensionless fitting parameters that are constant with respect to time and ψ_0 is again interpreted as the scour shape factor for the initial bed. Fig. 4.12(b) demonstrates that the scour shape factor increases systematically during backfilling, but most intensely for the smaller holes.

4.5.4 Coupled approaches

The development equations for the scour depth (4.14) and the scour volume (4.15) can be used to model the development of the scour depth and the scour volume independently of each other. Alternatively, the equations can be coupled through the definition of the scour shape factor (4.6) and either the scour depth or volume equation can be traded for a development equation for the scour shape factor. Below, I present this coupled approach in four combinations and assess the volume-based general approach and the depth-based similarity approach subsequently.

General approaches The general approaches recognize that the scour shape factor varies in time and come in two flavors depending on which supplementary development equation is adopted:

- *Depth-based* general approach that determines the scour volume from (4.6), (4.16) and (4.14).
- *Volume-based* general approach that determines the scour depth from (4.6), (4.16) and (4.15).

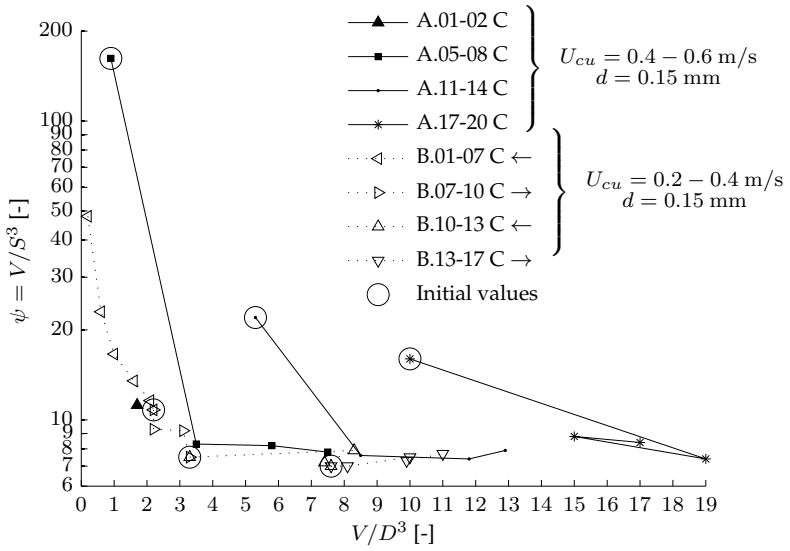

(a) Scouring

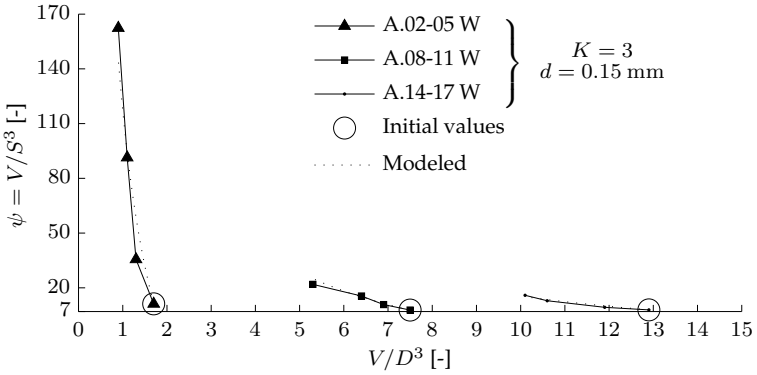

(b) Backfilling

Figure 4.12 *Measured development of scour shape factor.*

C or W denote current or waves, respectively.
The arrows denote the current direction in tidal runs.

Similarity approaches The experiments clearly demonstrate that the scour shape factor varies in time. Nevertheless, it can be useful to apply the approximation of geometrical similitude in which the scour shape factor is taken as constant with respect to time. Such a similarity approach relies on (4.6), (4.7) and a development equation for either the scour volume or the scour depth. Based on the choice of the latter relation, I envision two flavors of similarity approaches:

- *Depth-based* similarity approach that determines the scour volume from (4.6), (4.7) and (4.14b). This readily implies that the scour volume develops as:

$$V = \psi\big(S_\infty + (S_0 - S_\infty)\, e^{-t/t_S}\big)^3 \tag{4.19}$$

- *Volume-based* similarity approach that determines the scour depth from (4.6), (4.7) and (4.15). By substituting (4.6) into (4.15b) and eliminating the constant-valued ψ, it can be seen that this variant of the similarity approach implies that the scour depth develops as:

$$S = \Big(S_\infty^3 + (S_0^3 - S_\infty^3)\, e^{-t/t_V}\Big)^{1/3} \tag{4.20}$$

The qualitative resemblance between each pairs of (4.15b),(4.19) and (4.14b),(4.20) is striking. Quantitatively, the equations of each pair also agree. I have obtained some universal results in two special cases, namely scouring from a plane bed ($S_0 = 0$) and backfilling to a plane bed ($S_\infty = 0$). In the first case, a least square analysis at evenly spaced time stations in the interval $t \in [0; t_V]$ demonstrates a reasonable agreement when using $t_V/t_S \approx 2.4$ or $t_V/t_S \approx 3$ for the depth-based or volume-based similarity approach, respectively. The former choice is illustrated in Fig. 4.13 where the volume-based approach is shown with solid curves. In the second special case, when $S_\infty = 0$, the equations of each pair remarkably become *identical* when using $t_V/t_S = 1/3$. For example, (4.14b) reduces to $S_0 \exp(-t/t_S)$ and (4.20) reduces to $S_0 \exp(-t/(3t_V)$. In other than these special cases, it appears that an individual analysis must be made.

The above analyses have several implications. First, assuming that scour holes develop in a geometrically similar way during

scouring, the experimental support for (3.1) can be taken as indicative support for the scour volume equation (4.15) during scouring. Secondly, the formula for t_S during scouring and the above relations for t_V/t_S can be used to estimate t_V. This is useful at the moment since the time scale formula (3.2) and the auxiliary formulas for t_S^* in Table 3.1 cover a wider range of conditions than the present experiments. The use of the conversion factors is assessed in the following section and indicates a fair agreement during scouring. Finally, these results indicate that the two similarity approaches give nearly the same results for a suitable choice of t_V/t_S. Thus, if one decides to adopt a similarity approach for an approximate scour forecast, one can freely choose between either variant.

4.5.5 Assessment

I want to close this legacy with an assessment that takes its point of departure in the experimental runs of series A and the decisions that a designer will face in making a scour forecast. Specifically, I investigate the following questions:

- *Should one rely on the volume-based general approach or the depth-based similarity approach of Sec. 4.5.4?* The first choice fits best with the experiments, as we will see, but the latter choice may be attractive because it is conventionally used during scouring and avoids bathymetry techniques.
- *In a depth-based similarity approach, what is a good choice of the scour shape factor during both scouring and backfilling?*

To answer these questions, I have shown the measured and modeled parameter development in runs A.01-18 in Fig. 4.14. In the experiments, global erosion appears at $t = 91\ \mathrm{min}$ in the order of $1\ \mathrm{cm}$ and grows even larger for $t > 151\ \mathrm{min}$. Therefore, the runs beyond the latter time station have not been considered further. The model curves denoted by $S(t)$, $V(t)$ or $\psi(t)$ refer to (4.14), (4.15) or (4.16), respectively. If two symbols are given, such as $S(t), \psi(t)$, the determination of the third unknown relies on the definition of the scour shape factor (4.6) as discussed in Sec. 4.5.4. The parameter values are given in Table 4.2 based on Ref. 1 and some preliminary fits for the present purpose. Importantly, the parameters have been constrained such that all scouring runs share values and likewise all backfilling runs share values. The model equations have been

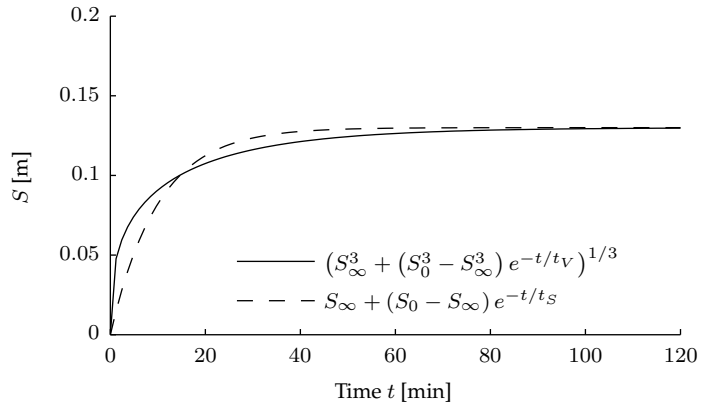

(a) Scour depth development

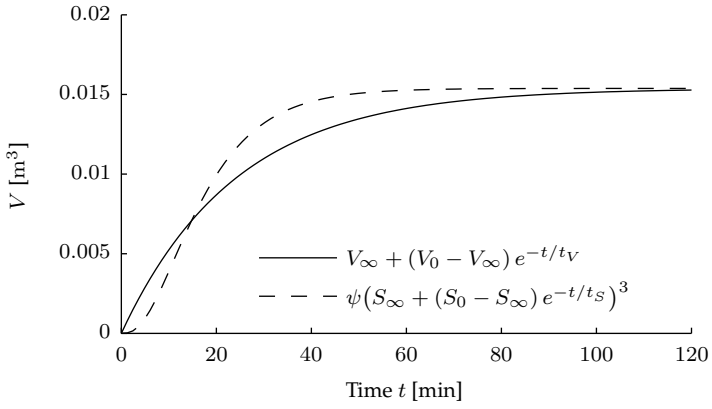

(b) Scour volume development

Figure 4.13 *Parameter development using two similarity approaches for scouring from plane bed.*

Illustrated with $S_0 = 0$, $S_\infty = 0.13$ m, $\psi = 7$ and $t_V/t_S = 2.4$.

solved in their ODE formulation with a forward Euler scheme with the initial conditions $V_0 = S_0 = 0, \psi_0 = 1000$.

Fig. 4.14 shows that the volume-based general approach provides an excellent fit of the scour volume and scour depth. There is a small deviation in the scour depth in the first branch of backfilling at $t \in [1\ \mathrm{min}; 31\ \mathrm{min}[$ where the scour depth is slightly over-estimated. This stems from the corresponding under-estimation of the scour shape factor as shown in Fig. 4.14(b). This, in turn, stems from a subtle over-estimation of the magnitude of the scour volume rate.

Over-all, the scour depth equation (4.14) provides a good fit for the scour depth as shown in Fig. 4.14(c). However, the scour depth equation completely fails in modeling the first branch of backfilling. Here, the innate behavior of the scour depth equation assumes the *weakest* magnitude of the scour depth rate since the hole is close to equilibrium as discussed previously in connection with Fig. 4.11. In contrast, the experiments show that the scour depth rate has the *strongest* magnitude here in comparison to all the considered backfilling runs. This is consistent with the observed development of the scour geometry and the hypothesized physical process of sediment dispersion and more uniform deposition around the pile during backfilling as discussed in Sec. 4.3. These considerations strongly suggest that *the principal development of the scour depth equation* (4.14) *can be incompatible with the measured development*. A more appropriate explicit formulation of the scour depth could simply be a line with constant slope rather than exponential decay. This further questions the meaningfulness of using the scour depth time scale t_S for the scour process because the time scale of scouring may no longer be comparable to the 'time scale' of backfilling. In these experiments, the scour depth equation passes the practical test since the deviation in the first branch of backfilling is acceptable for this small hole and the equation captures the second branch of backfilling at $t \in [38\ \mathrm{min}; 68\ \mathrm{min}[$. But under other conditions, we may not be so lucky. The consequence of the failure in representing the strong magnitude of the scour depth rate during backfilling is that the scour depth is over-estimated. This reduces the apparent cost-potential of a scour-exposed design.

Adopting a depth-based similarity approach, the scour depth equation has been used together with a constant-valued scour shape factors $\psi = 7.5$ and $\psi = 15$ to estimate the scour volume development. Aside from the under-estimation of the scour vol-

ume at the first branch of backfilling, the two model curves nearly envelope the measured development of the scour volume. This is attractive but, as a penalty, the envelope is broad.

An inspection of the values for t_V/t_S from Table 4.2 shows that $t_V/t_S = 9.5/4.6 \approx 2.1$ during scouring. This is approximately consistent with the theoretical value for a depth-based similarity approach as given in Sec. 4.5.4, i.e. $t_V/t_S \approx 2.4$. During backfilling, however, there is a large discrepancy between the actual $t_V/t_S \approx 1.9$ and the theoretical similarity-approach value of $t_V/t_S = 1/3$. These results are consistent with the observation that the scour holes are approximately geometrically similar during most of the scouring process but are dissimilar during the backfilling process.

The normalized time scale t_S^* for current-scouring is within the predicted range of the corresponding formula in Table 3.1 as detailed in Sec. 6.1.3 of Ref. 1 and thus supports the conventional time scale formula at model-scale. To investigate its validity at field-scale, the present results are scaled to field-size in the following thought-exercise for the backfilling runs. First, temporarily assume that the normalized time scale t_V^* is only a function of K and ζ'_{r_∞} as suggested for wave-scouring in Table 3.1. Then, a field-case with the same parameter values as in the present tests, i.e. $K = 3$ and $\zeta'_{r_\infty} = 0.2$, would also experience $t_V^* = 5.0$. Thirdly, insert this into the time scale formula (3.2) while taking the remaining values as in the present tests, i.e. most notably $d = 0.15\ \mathrm{mm}$ and $s = 2.65$. The remarkable result of this exercise implies that the time scale for the scour volume development is $t_V \approx 125\ \mathrm{days}$ at field-scale. This appears to be unrealistically large and therefore suggests that either additional parameters influence the normalized time scale t_V^*, the time scale formula does not scale correctly or the present results are not representative. For the up-scaled current-scoured runs, this results in $t_V \approx 11\ \mathrm{days}$ at field-scale which also appears to be overestimated.

In conclusion, these considerations entail that I recommend the volume-based general approach because it provides an accurate description of the scour depth and scour volume during scour and backfilling. The designer can also settle with adopting the depth-based similarity approach with the awareness that it may overestimate the scour depth during backfilling for the smaller holes and give an uncertain estimate of the scour volume development.

Finally, I note two critique points that have been raised by existing researchers. Firstly, the branches of these tests do not each reach a state of equilibrium and therefore the accuracy of the equilibrium value V_∞ and the time scale t_V has been questioned. I answered this critique in Sec. 5.5 of Ref. 1. The defense is that the scouring or backfilling branches share parameters and the computed confidence limits on t_V and V_∞ implicitly estimate the mutual sensitivity as shown in Table 4.2. A second critique is the low sampling period of the bed measurements, which is 10 minutes in case of most backfilling tests. I respond to this here by emphasizing that these development equations are filtered and do not purport to capture the influence of oscillations at higher frequencies. In my opinion, this answers the critique satisfactorily. Instead, the main weaknesses of this framework, as I see it, are the limited number and impaired circumstances of the present experiments. The present findings should therefore be taken with some reservation until future studies have reviewed them.

* * *

Table 4.2 *Parameter values for modeled curves.*

Group	Property			Scouring	Backfilling
Load conditions	Normalized water depth	H/D	[–]	3	3
	Keulegan-Carpenter number	K	[–]	∞	3
	Characteristic fluid velocity	U_{cu}, U_m	[m/s]	0.5 ± 0.1	0.2
	Undisturbed Shields number	$\zeta'_{r\infty}$	[–]	0.2 ± 0.1	0.2
Scour volume ODE	Normalized scour volume	V_∞/D^3	[–]	13.7 ± 0.7	$0.1\,[0; 1.3]$
	Time scale for scour volume	t_V	[min]	9.5 ± 1.2	113 ± 18
	Normalized time scale	t_V*	[–]	0.42 ± 0.05	5.0 ± 0.8
Scour depth ODE	Normalized scour depth	S_∞/D	[–]	1.23 ± 0.1	0.2
	Time scale for scour depth	t_S	[min]	4.6 ± 1.3	60
	Normalized time scale	t_S*	[–]	0.20 ± 0.06	2.6
Scour shape factor ODE	Parameter 1	t_ψ, c_1	[–]	$t_\psi = 0.1$ min	$c_1 = 250 \pm 81$
	Parameter 2	ψ_∞, c_2	[–]	$\psi_\infty = 7.5$	$c_2 = 1.9 \pm 0.1$

The plus-minus for $V_\infty, t_V, t_V^*, S_\infty, t_S, t_S^*, c_1$ and c_2 are based on approximate 84% confidence limits as detailed in Ref. 1.
The pile diameter is $D = 0.10$ m.

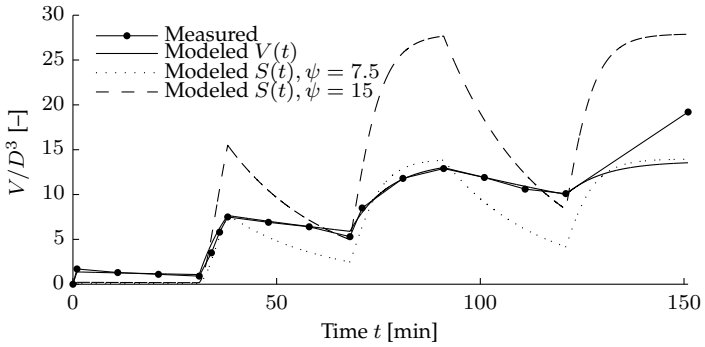

(a) Scour volume.

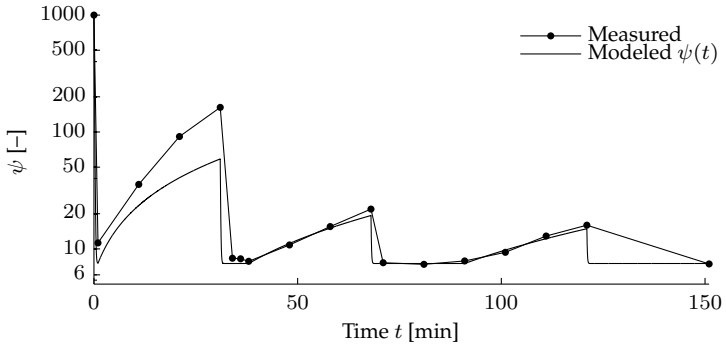

(b) Scour shape factor.

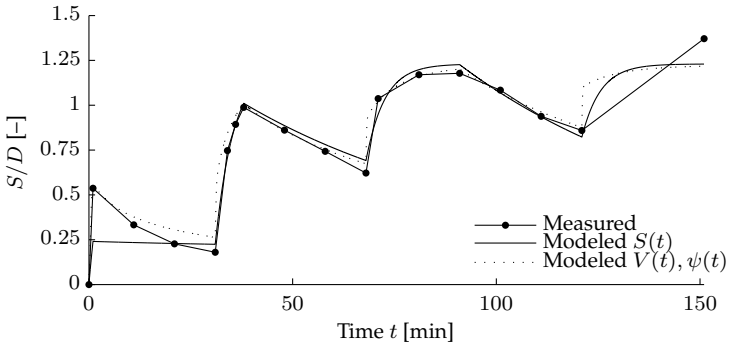

(c) Scour depth.

Figure 4.14 *Measured and modeled parameter development.*

Chapter 5

Legacy II: The Reverse Approach

In this chapter, I present my second contribution, namely the *reverse approach* that deals further with the second research question, i.e.:

How do the parameters develop in time for a given sea state?

This was answered partly in the previous chapter for *some* configurations but not for many other field-relevant configurations, say a wide range of Keulegan-Carpenter numbers K or for larger pile diameters D. The preceding treatment sparked two new sub questions:

- *Is the scour volume equation* (4.15) *valid for scouring and backfilling in other configurations?*
- *What are the parameters of the development equations, say the scour volume time scale t_V, for other configurations?*

Until these sub questions have been answered satisfactorily, the volume-based general approach should not, and in fact cannot, be applied for a general scour forecast.

One obvious way of answering these sub questions is to conduct further *experimental* studies as the present ones in the laboratory. Alternatively, one can conduct the experiments in the field. Finally, one can increase the level of detail and undertake *numerical* studies that mimic the interaction between the bed surface, fluid flow and

the sediment transport as done in Roulund et al. [2005]. The latter is illustrated as a *forward approach* in the interaction triangle of Fig. 5.1. Such additional studies would be quite valuable but also have some weaknesses.

Firstly, scour studies are time-consuming in case of scouring and are expected to be retarded further during the process of backfilling. As seen from Table 4.2, the present experiments suggest a ten-fold retardation when going from scouring to backfilling with respect to the scour volume development. Therefore, scour studies can only investigate the influence of a few recognized parameters. Secondly, the monopiles for offshore wind parks are so large that they cannot at present be treated in full scale in the laboratory or computers. This is due to present limitations in laboratory facilities[1]or computational resources[2], respectively. A typical length ratio between model and field is 1:50, as in the present experiments or Roulund et al. [2005]. Therefore, the hard-earned results will only be indicative for field-scale configurations due to the open possibility of scale effects.

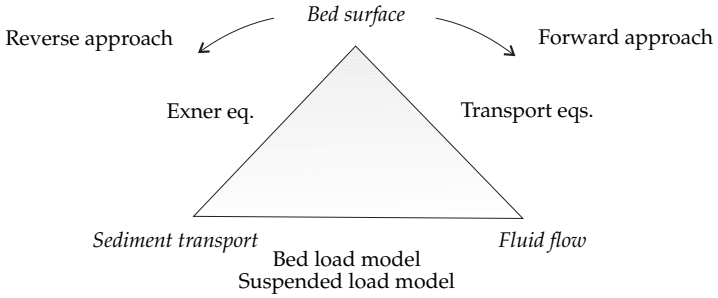

Figure 5.1 *Schematized interaction between bed surface, fluid flow and sediment transport.*

In this chapter, I present a variant of the numerical simulations above, namely the *reverse approach*. The reverse approach also relies on the interaction triangle but has the distinctive features that the point of departure is mainly a *prescribed scour geometry development* and the remaining items in the interaction triangle are determined *in a retrospective manner* as shown in Fig. 5.1. Refs. 3–4 establish a link between the scour geometry development in terms of $(dS/dt, dV/dt)$ and the bed elevation rate $\partial h/\partial t$. Ref. 4 establishes

the remaining links in between the bed elevation rate $\partial h/\partial t$ and the fluid flow in terms of the two-dimensional vector field for the mean bed shear stress τ'_α, written with two-dimensional index notation.

If we for a moment park the concern of the validity of the above links and return to it later in Sec. 5.2.2 and Sec. 5.4, we can see the potential of the reverse approach. It empowers us to estimate the field of bed shear stress for a given scour geometry development without actually having to carry out an experimental or numerical flow study. This allows one to more easily perform parametrical studies and identify the combinations of governing input parameters, say $(t_V, D, \ldots)$, that produce nearly the same spatial distribution of the amplification of bed shear stress magnitude relative to the far-field magnitude. The combinations of parameters can be compared to those of the time scale formula (3.2) and if necessary lead to the development of an improved formula. The studies can even range up to field-scale and provide *some indications* of the scaling of t_V at field-scale. Thus, *parametrical studies based on the reverse approach appear to facilitate quicker and more comprehensive* indicative *answers to the above sub questions than the laboratory or numeric scour studies*.

Besides the concept and demonstration of the reverse approach, I have also made two distinct contributions within the approach. First, I have detailed and benchmarked a procedure for treating local sliding of grains. Secondly, I have postulated a new formula for sediment entrainment. These contributions will be outlined in this chapter.

In the first three sections, I expose the assumptions of the method by reviewing the interaction triangle that the reverse approach is partly based on, present the chosen governing equations and recapping the solution strategy. In the final section, Sec. 5.4, I compare the estimated shear stress of the reverse approach with a numeric study and discuss the performance. I conclude that the prediction in the reverse approach needs to be improved and validated further before it can be applied in parametric studies.

5.1 Interaction triangle

The interaction triangle is the state-of-the-art method for simulating sediment transport and has been used in e.g. Brørs [1999] or Roulund et al. [2005]. The representation of a *triangle* is inspired

from Umeda et al. [2008] but the ideas in the framework are reported elsewhere, e.g. Rijn [1985]. Conceptually, the interaction triangle relies on a division of space into three regions but in practice, the interfaces between the regions can be difficult to define as illustrated in Fig. 5.2. The three regions are outlined below:

- *Seabed* dominated by still grains in a skeleton. The elevation at the top of the seabed is h.
- *Bed load layer* dominated by coarser grains in nearly continuous mutual contact by sliding, rolling or jumping. The grains in this region are referred to as bed load. The elevation at the top of the bed load layer is z_b.
- *Suspended load layer* dominated by finer suspended grains that are referred to as suspended load. The elevation at the top of the suspended load layer is z_s, corresponding to the free surface of the fluid.

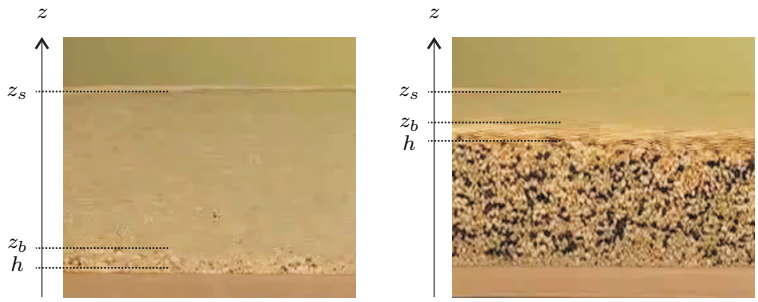

Figure 5.2 *Snapshot photos of sediment transport and regions at two different moments during a live-bed flume test.*

Adopted from Gough [2007].

Besides the three regions, the interaction triangle also considers three components, namely the bed surface, fluid flow and sediment transport as shown earlier in Fig. 5.1. The components are coupled with the following three links:

- *Transport equations for the fluid flow:* The mixture of fluid and sediment extends from the seabed to the free surface, covering both the bed load and suspended load layers. In typical

computational studies, the bed surface is taken as impermeable and the mixture is modeled as a conventional Newtonian fluid whose transport equations for fluid mass and momentum are solved. The Newtonian assumption ignores the influence of the immersed grains, except for perhaps allowing changes in bulk fluid properties such as the density or dynamic viscosity when the grain concentration changes locally. Bagnold [1954] demonstrated that as the interaction between grains mutually and with the fluid becomes stronger, the Newtonian assumption becomes cruder. This can be the case in the bed load layer but is usually not treated.

- *Bed/Suspended load models:* The fluid flow is related to the sediment transport through transport models for the bed load and suspended load. Typically, these models operate on filtered quantities that have been smoothed in time and space. The sediment transport can be quantified in terms of the filtered volumetric fluxes per unit width, namely $Q_\alpha \equiv \int_{z_1}^{z_2} C U_{d\alpha}\, dz$ where C is the filtered volumetric grain concentration, $U_{d\alpha}$ is the filtered sediment velocity and the limits z_1, z_2 are the bottom and top elevations of the respective layers. In scour studies, the sediment transport models can be based *directly* on the fluid flow by resolving an additional transport equation for C, adopting the velocity of the fluid for the sediment, i.e. $U_{d\alpha} \approx U_\alpha$, and using the flux definitions. Alternatively, the models can be based *indirectly* on the flow, e.g. in terms of the filtered bed shear stress associated with skin friction τ'_α, and employ empirical or theoretical relations to determine the corresponding sediment fluxes. I have adopted the latter approach for both the bed load and suspended load. As an approximation, it is also common practice to neglect either the bed load or suspended load.
- *The Exner equation:* The sediment transport is related to the bed surface through the Exner equation that expresses continuity of sediment mass or volume. Depending on which models for the bed load and suspended load that are adopted, the entrance into the Exner equation can vary.

5.2 Governing equations

In this section, I outline the governing equations that have been implemented in the reverse approach. I begin with the Exner equation, proceed with the model for the bed elevation rate and conclude with the transport models for the bed load and suspended load. Of these, I elaborate the model for the bed elevation rate and the model for the suspended load that have emerged from this research.

5.2.1 Exner equation

Consider a control volume that extends from the top of the bed load layer and well down into the bed and has infinitesimal horizontal extent. Assuming that the bed material is incompressible, the Exner equation expresses the conservation of mass or volume of the bed material inside the control volume:

$$-C_h \frac{\partial h}{\partial t} = \frac{\partial Q_{b\alpha}}{\partial x_\alpha} + e \tag{5.1}$$

In the equation, $\partial h/\partial t$ is the bed elevation rate, C_h is the volumetric grain concentration in the bed, $Q_{b\alpha}$ is the bed load flux and e is the entrainment rate related to the suspended load. The Exner equation mimics that the bed elevation in the control volume decreases either due to an increase in the bed load flux from one position to another (more precisely, due to a non-zero divergence $\partial Q_{b\alpha}/\partial x_\alpha > 0$) or due to grains being entrained from the control volume into suspension ($e > 0$). The grain concentration in the bed C_h accounts for the effects of porosity and is assumed to be constant.

5.2.2 Bed elevation rate

In this section, I outline the components and performance of the model of Ref. 3 for describing the bed elevation rate $\partial h/\partial t$ in the scour domain. The model is used onwards in Ref. 4 that modifies it slightly in the scour domain and estimates the bed elevation rate in the remaining bed domain if these modifications are needed.

The model in Ref. 3 mainly operates on *rates*, such as the bed elevation rate $\partial h/\partial t$, scour depth rate dS/dt and the scour volume rate dV/dt. This has at least two advantage. Firstly, this allows

the model for the bed elevation rate to be relatively simple and yet it can be integrated with respect to time to accommodate a more complicated bed development. In pictures, the procedure of integrating the bed elevation rate can be viewed as superimposing the surfaces of the bed elevation rate as shown in Fig. 5.3 on top of each other at each time step so as to produce a more general accumulated bed surface. The second advantage of such a rate approach is its simplicity since the bed elevation rate enters directly into the Exner equation (5.1).

The model consists of two components that are invoked in serial at each time step:

- *Predictor* that mainly enforces the prescribed scour geometry development.
- *Corrector* that enforces local sliding where the slope angles exceeds the repose angle. This component is optional and, when enabled, is carried out before the predictor.

In the following outline of the components, I will usually omit the distinction between the predictor and the corrector in the text due to readability.

Predictor The bed elevation rate is taken as the following parametrized two-dimensional surface:

$$\left(\frac{\partial h}{\partial t}\right)_{\text{pre}} = b \cdot (1 - r_2^p)^{1/p} \tag{5.2}$$

where b is the bed elevation rate at the pile base, p is a curvature coefficient and r_2 is a normalized radius. The normalized radius is:

$$r_2\left(r, \theta, t\right) = \frac{r - r_{\min}}{r_{\max}\left(\theta, t\right) - r_{\min}} \tag{5.3}$$

where $r_{\min} = D/2$ is the outer radius of the pile and $r_{\max}$ is the outer radius of the scour domain. This formulation delegates the following roles to the coefficients:

1. The radius of the outer boundary $r_{\max}$ determines the *outer extent of the domain* of the surface. In Ref. 3, it is formulated such that the outer boundary resembles a semi-circle in the upstream domain and a semi-ellipse in the downstream domain. This allows the entire scour domain to be shaped both

as a circle and droplet as observed during scouring and backfilling, respectively, in Fig. 4.7. An example of the modeled droplet-shaped domain is illustrated in Fig. 5.3 and can be seen most clearly for $p \geq 1$. The parameters that define $r_{\max}$ are prescribed and in the present formulation, the outer extent of the scour domain is dictated by the scour depth rate during scouring and is assumed to remain constant during backfilling.

2. The base elevation rate b determines the *sign of the surface* and the *shape along the pile perimeter*. It is related to the prescribed scour depth rate $(dS/dt)_{\text{pre}}$ of an integral definition. In general, b can vary with the angle but if a uniform shape is chosen, the base elevation rate must be computed as $b = -(dS/dt)_{\text{pre}}$. Fig. 5.3 illustrates such an uniform case during backfilling $(b > 0)$.
3. The curvature coefficient p determines the *shape of the surface*. It controls the curvature of the curve that can be drawn in radial direction between the surface at the pile perimeter and the outer boundary. The curvature coefficient can range between $p \in]0; \infty[$ and the two asymptotic limits correspond to the cases where the normal vector to the surface at the pile perimeter is directed horizontally or vertically, respectively. This is also seen in Fig. 5.3. The curvature coefficient p is tuned so as to ensure that the volume of the surface equates the prescribed scour volume rate $(dV/dt)_{\text{pre}}$.

Corrector The corrector was inspired by the sliding models of Roulund et al. [2005], Roulund [2000] and Umeda et al. [2006]. Unfortunately, their model descriptions were only conceptual or unclear, so in Ref. 3 I clarified how the approach is implemented in practice and also compared it to the present experiments.

In brief, the slope angle is computed at every point of the bed domain before the predictor step. If the slope angle of the current bed surface exceeds the repose angle anywhere and the corrector is enabled, the corrector step is carried out. The corrector ensures that the bed elevation is changed locally where the slope angle is exceeded such that the bed material slides down the steepest slope. In practice, this is done conveniently by using the Exner equation (5.1) since it inherently conserves the mass or volume of the bed

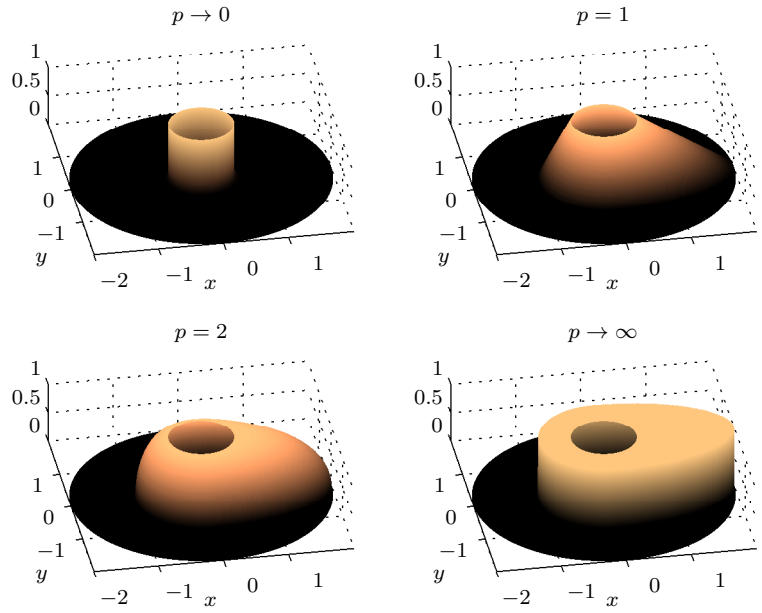

Figure 5.3 *Examples of bed elevation rate $(\partial h/\partial t)_{pre}$ in scour domain.*

Backfilling ($b > 0$) for a droplet-shaped domain, constant-valued base elevation rate ($\partial b/\partial\theta = 0$) and different constant values for the curvature coefficient p.

material. In an inner loop, a temporary sediment flux is computed $Q_{b\alpha}$, the entrainment rate is temporarily taken as nil ($e = 0$) and the bed elevation rate $\partial h/\partial t$ from the Exner equation is integrated numerically with respect to time for one inner time step. The steps are repeated until the slope angle of the updated bed surface is everywhere less than the repose angle. Outside the corrector, these bed changes appear to have occurred instantaneously.

Assessment To expose the performance of this model, I compared it with the present experiments in Ref. 3. To do so, the initial bed surface is taken from one of the experiments and the parameters of the development equation are prescribed. Then, the bed elevation rate $\partial h/\partial t$ is integrated numerically with respect to time and h is extracted at the same time stations as the experiments. Fig. 5.4 shows a comparison for runs A.05-11. The figure suggests that the measured and modeled bed surface within the scour domain agree

qualitatively. In all of the runs, the difference in bed elevation at points located inside the scour domain is on average 6 % of the pile diameter. The comparison also revealed that the corrector component was necessary to capture the development of the upstream slope during scouring as seen in Fig. 5.4(a).

Overall, the model appears to perform satisfactorily. However, it is important to recognize that *the bed elevation rate $\partial h/\partial t$ of the model is filtered in time and space.* This is because it is based on few snapshots of the bed surface during the experiments that cannot convey the detailed history of the bed development. For example, an oscillation can be superimposed on the development equations and still give the same mean development. Or the scour depth rate and scour volume rate can both be satisfied simultaneously by a multitude of surfaces for the bed elevation rates. Consequently, although the model performs well for the overall development, it may not succeed in modeling an instantaneous state. As suggested in Sec. 5.4, this very component of the reverse approach may be responsible for the poor prediction of the spatial distribution of the bed shear stress.

5.2.3 Bed load model

In the reverse approach, two bed load models were implemented in order to investigate their influence on the model prediction. The two bed load models were based on existing influential work:

- *Brørs model* mainly resembling that of Brørs [1999]. This can be viewed as a simple approach and variants of this are also used in Umeda et al. [2006, 2008] and Liu and García [2008].
- *Roulund model* mainly resembling that of Roulund et al. [2005] and Engelund and Fredsøe [1976]. This can be viewed as an elaborate approach.

Both of the present bed load models operate on the two-dimensional vector field of the *mean* bed shear stress τ'_α. It appears that suitable turbulent correlations can be included to improve the model performance in turbulent flows as will be the case for the scour around monopiles. Bed load equations that include turbulent correlations are suggested in Sumer et al. [2003]. Consequently, this implies that the reverse approach can only estimate τ'_α in the present implementation but may be extended in future to estimate

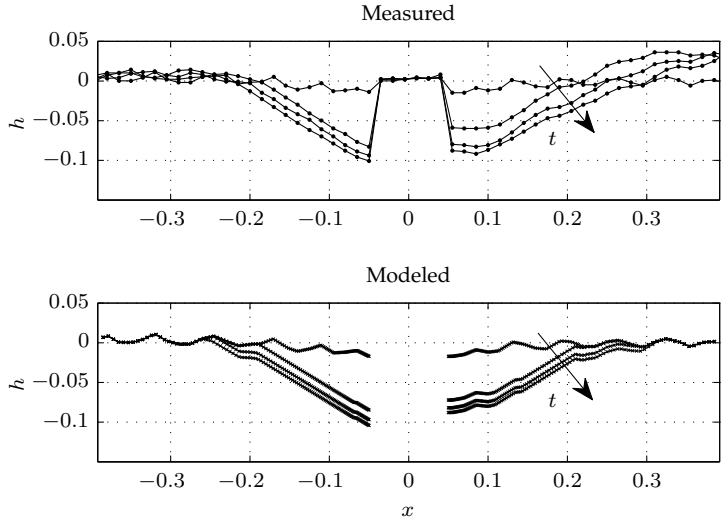

(a) Scouring A.05-08.

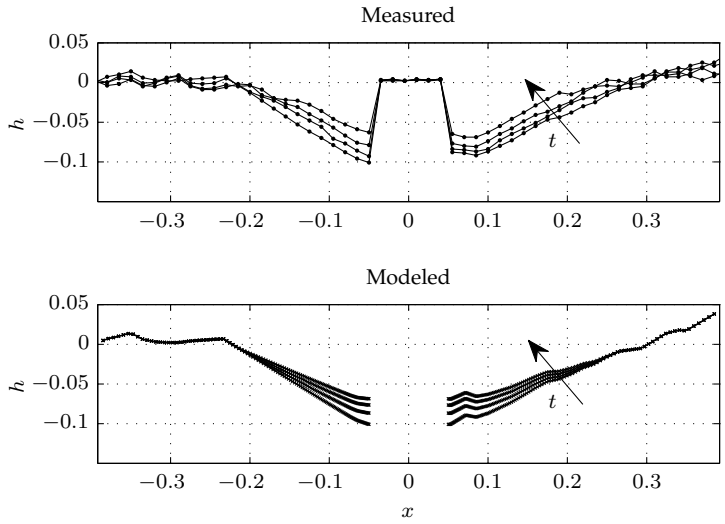

(b) Backfilling A.08-11.

Figure 5.4 *Measured and modeled bed surface development.* All dimensions in meter. The arrows indicate increasing time.

the corresponding turbulent correlations. In the following, I will briefly present the Brørs model.

Brørs model The bed load flux $Q_{b\alpha}$ is taken as:

$$Q_{b\alpha} = \begin{cases} Q_{b0} \cdot \left(\dfrac{\tau'_\alpha}{\tau'} - c_Q \dfrac{\partial h}{\partial x_\alpha} \right), & \zeta' > \zeta_c \\ 0, & \text{else} \end{cases} \tag{5.4}$$

where Q_{b0} is the bed load intensity, c_Q is a slope coefficient, τ'_α is the mean bed shear stress vector with the magnitude τ' and finally, ζ' and ζ'_c are the local and critical Shields numbers. The slope coefficient is prescribed and $c_Q \neq 0$ ensures that the bed load travels somewhere between the directions of the bed shear stress τ'_α and the steepest slope, i.e. $-\partial h/\partial x_\alpha$. The critical Shields number is computed such that it includes the influence of the bed slope as detailed in Ref. 4. The bed load intensity Q_{b0} corresponds to the magnitude of the bed load flux in case of plane bed and is taken from Nielsen [1992, Sec. 2.3.4]:

$$Q_{b0} = 12 \ \left(\zeta' - \zeta_c\right) \sqrt{\zeta'} \sqrt{(s-1) g d^3} \tag{5.5}$$

Other models for Q_{b0} instead of (5.5) are also commonly used, e.g. Engelund and Fredsøe [1976] or Meyer-Peter and Müller [1948].

5.2.4 Suspended load model

In Ref. 4, I developed and briefly assessed a model for the entrainment rate e that enters into the Exner equation (5.1). The development has been inspired partly by Garcia and Parker [1991], Rijn [1985] and Engelund and Fredsøe [1976] and is presented below.

Based on the Reynolds-averaged transport equation for the grain concentration of the incompressible suspended grains and assuming that the mean vertical fluid velocity W is negligible near the presumingly impermeable bed, the entrainment rate can be determined as:

$$e = -C_b W_d + \overline{\tilde{c}\tilde{w}}(z = z_b) \tag{5.6}$$

Here, C_b is the mean grain concentration in the bed load layer, W_d is the terminal settling speed of the sediment and $\overline{\tilde{c}\tilde{w}}(z = z_b)$ is a turbulent correlation that I call the *entrainment correlation*. The

entrainment correlation is the Reynolds-average of the product of the fluctuating grain concentration $\tilde{c}$ and the fluctuating upward fluid velocity $\tilde{w}$ where the fluctuations are evaluated at the same point at the elevation z_b. In Ref. 4, I postulate the following new model for the entrainment correlation:

$$\overline{\tilde{c}\tilde{w}}(z = z_b) = c_e C_b U'_f \tag{5.7a}$$

Above, U'_f is the friction velocity associated with skin friction and c_e is a dimensionless coefficient that I call the *equilibrium coefficient*. In this model, C_b and U'_f are assumed to be the governing quantities for characterizing the entrainment correlation. The friction velocity U'_f is retained since it is assumed to be proportional to the total friction velocity U_f and the latter is known to characterize the intensity of the fluctuation $\tilde{w}$ in the inner region of simple boundary layers in the limit of infinite Reynolds number [George, 2007], i.e. $U'_f \propto U_f \propto \sqrt{\overline{\tilde{w}^2}}$. The mean grain concentration is retained based on the hypothesis that the inertia of the grains is relatively weak so the turbulent eddies will convect the available grains at a particular point. Depending on whether there are few or many grains available, on average, the fluctuation $\tilde{c}$ is expected to vary weakly or strongly, respectively, i.e. $\sqrt{\overline{\tilde{c}^2}} \propto C_b$. The equilibrium coefficient c_e is taken as:

$$c_e = \frac{W_{de}}{U'_{fe}} \tag{5.7b}$$

where the subscript e denotes values in the *equilibrium situation*, i.e. $e = 0$. This choice ensures that the entrainment correlation (5.7) satisfies the *equilibrium condition* in the equilibrium situation, i.e. $\overline{\tilde{c}\tilde{w}}(z = z_b, e = 0) = C_{be} W_{de}$.

Aside from satisfying the equilibrium condition, the present model lends empirical support in the equilibrium situation in two further respects. First, (5.7b) can be interpreted as the condition for the onset of entrainment. As such it strongly resembles the existing criteria of the type $c_{e2} = W_d/U'_f$ where the constant is taken as $c_{e2} = 0.8$ in Engelund and Fredsøe [1976] or $0.25 < c_{e2} < 1$ as summarized in Rijn [1984b]. Secondly, the prediction of the present model is comparable to existing models. Fig. 5.5 shows an example of the entrainment correlation as function of transport stage for a plane bed in the equilibrium situation ($\Rightarrow C_b = C_{be}$). The illustrated models are Dey and Debnath [2001], Rijn [1984d], Garcia and

Parker [1991] and the present (5.7a). In the latter two models, the equilibrium grain concentration C_{be} is computed from one of three different formulas. The formulas are denoted by Br, Ro or Ri and correspond to that of Brørs [1999], Engelund and Fredsøe [1976] or Rijn [1984b]. The present model has been shown with $c_e = 0.4$.

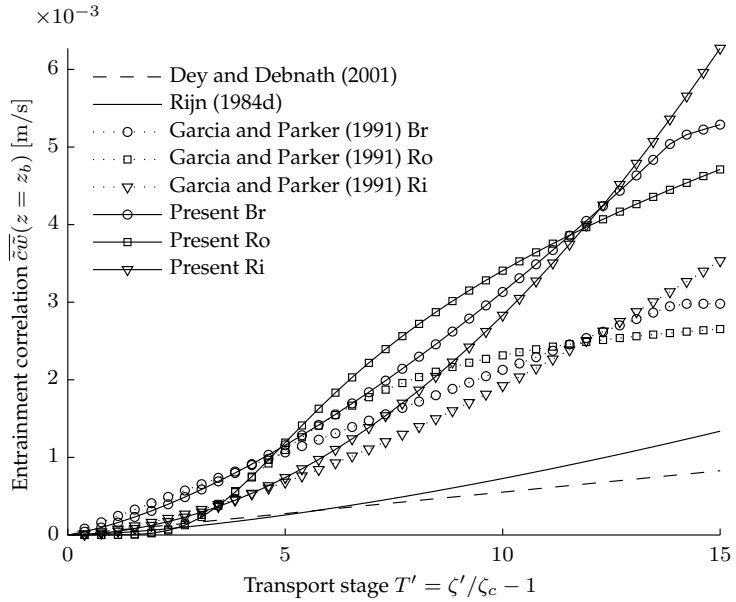

Figure 5.5 *Entrainment correlation as function of transport stage in the equilibrium situation.*

In the present implementation, the equilibrium friction velocity U'_{fe} is determined such that it enforces particular conditions at the outer boundary of the bed domain, namely zero entrainment rate during current or zero *phase-averaged* entrainment rate during waves. Furthermore, two approximations are applied. First, the settling speed is taken for a solitary grain and is thus assumed to be independent of the grain concentration, implying $W_{de} \approx W_d$. Secondly, the grain concentration is computed from an equilibrium formula by adopting a *grain concentration approximation* in a general case, i.e. $C_b \approx C_{be}$. The two approximations imply the following approximate entrainment rate:

$$e \approx W_{de} C_{be} \cdot \left(\frac{U'_f}{U'_{fe}} - 1 \right) \tag{5.8}$$

Equation (5.8) is used onwards for the entrainment rate in the reverse approach. The equation demonstrates that *the present model has the ability to simultaneously satisfy the equilibrium condition and use the grain concentration approximation without erroneously predicting* $e = 0$ *always.* Consequently, the present model allows one to avoid the computational overhead of solving a transport equation for C and evaluating the solution at z_b to obtain C_b. This ability appears to be unique to the present model in comparison to common existing models. For example, the model $e = -C_b W_{de} + C_{be} W_{de}$ of Garcia and Parker [1991] yields $e = 0$ always if the first term is approximated using $C_b \approx C_{be}$. The model of Brørs [1999] is based on the concept of eddy viscosity ν_t and with minor modifications, it can be interpreted as $e = -W_{de} C_{be} - \nu_t \partial C / \partial z$. If the eddy viscosity of equilibrium channel flows and the Rouse concentration profile are adopted in general, this model becomes identical to the model of Garcia and Parker [1991] and also predicts $e = 0$ always. Alternatively, one might adopt other formulas as given by Dey and Debnath [2001] or those reviewed in Rijn [1984d] but these do not guarantee the equilibrium condition.

The main weakness of the present entrainment model appears to be the lack of comprehensive empirical or theoretical studies on its performance, *especially in more general situations than the equilibrium situation.*

5.3 Solution strategy

The solution strategy for the reverse approach is detailed in Ref. 4 and recapped briefly here. The preceding equations are used in a forward order to establish the boundary conditions and in the reverse order to establish the field conditions and resolve the field. The procedure for resolving the field involves the following six steps:

1. First, the grain concentration in the bed C_h is assumed to be known and constant with respect to time and space.
2. Secondly, $\partial h / \partial t$ is prescribed in the bed domain such that it resembles the model in Sec. 5.2.2 in the scour domain and approaches the undisturbed bed elevation rate at the outer boundary of the bed domain.

3. Now, the only remaining unknown in the Exner equation (5.1) is the bed load flux $Q_{b\alpha}$ since its divergence and the entrainment rate can both be considered to be functions of $Q_{b\alpha}$. To proceed, a guess $\hat{e}$ is made of the true field of the entrainment rate e such that the guessed entrainment rate approaches the undisturbed value at the outer boundary of the bed domain and satisfies a volume rate condition.
4. Fourth, the bed load flux is assumed to be irrotational so the Exner equation simplifies to the Poisson equation. By approximating the derivatives of the Poisson equation and its boundary conditions with finite differences, the resulting matrix equation can be solved and the bed load flux in the bed domain can be determined.
5. Fifth, since the bed load flux is now known, one of the bed load models can be used to determine the fields for the friction velocity U'_f. Next, the grain concentration in the bed load layer C_{be} can be determined using an equilibrium formula. Subsequently, the field of the entrainment rate can be computed by the approximate formula for the entrainment rate (5.8) and is denoted e_*.
6. Since the guessed $\hat{e}$ and computed e_* fields of the entrainment rate should be identical, steps 3–5 are repeated until acceptable agreement has been achieved.

5.4 Assessment

Using the reverse approach, I presented a preliminary parametric study in Ref. 4. In the following discussion, I mainly consider the scouring simulations denoted S14 and S41 in Ref. 4 for which existing results are available. The amplification of the local magnitude τ' compared to the far-field magnitude τ'_{ref} is shown in Fig. 5.6. The minimum and maximum amplification of the present simulations are shown in the color-bar and the scour holes extend beyond the shown domain.

The input of the two present simulations were identical except for the aspect that either the Brørs or Roulund model was adopted as bed load model. The simulations considered current-scouring from an initial scoured bed that was made artificially so as to resemble the measured bed of run A.08 shown in Fig. 4.7(b). The scour

geometry development was based on the volume-based general approach with the parameters of Table 4.2 with the exception that the time scale for the scour shape factor development was taken as $t_\psi = 1\,\mathrm{min}$. For comparison, the steady Reynolds-averaged study of Roulund et al. [2005, Sec. 6.2] is considered. This study treated the same pile diameter and comparable configurations of the scoured bed ($S/D \approx 1$, $L/D \approx 6.5$) and the sea state ($U_{cu} = 0.46\ \mathrm{m/s}$, $H/D = 2$). The large-eddy simulations of Zhao and Huhe [2006] for a somewhat comparable configuration were also considered but not shown here.

Fig. 5.6 demonstrates both the success and failure of the reverse approach. On one hand, the figure demonstrates the viability of the reverse approach and the present simulations appear to capture the correct order of magnitude of the bed shear stress amplification. On the other hand, a more careful inspection suggests that the reverse simulations fail to capture a critical aspect, namely the correct *spatial distribution* of the bed shear stress. Compared to Roulund et al. [2005], the present simulations predict a higher amplification in the *oblique zone* ($\theta \approx 3\pi/4,\ r/D = 0.5$) but a much lower amplification in the *crescent zone* ($\pi > \theta > 3\pi/4,\ 0.7 < r/D < 1.1$). The presence of the highest amplification in the crescent zone in Roulund et al. [2005], presumingly due to the presence of horseshoe vortices, is confirmed by Zhao and Huhe [2006] and consistent with the observed slope angles as argued previously in Sec. 4.3.3. Therefore, the discrepancy most likely *stems from poor approximations in the present implementation of the reverse approach*. As seen in Fig. 5.6, the discrepancy persists even when the bed load model is changed. It also persists when the formulation or parameters of the base elevation rate b of Sec. 5.2.2 was changed. Therefore, I suspect that the discrepancy originates from one or both of the following two assumptions:

- The formulation of the predictor bed elevation rate in (5.2) prohibits erosion/deposition to occur more intensely when going in a radial direction away from the pile.
- The bed load flux is assumed to be irrotational as mentioned in Sec. 5.3.

Therefore, *future research is encouraged to explore whether relaxing the above-mentioned assumptions can redeem the discrepancy*. Until this issue is resolved, it seems futile to proceed to the subsequent tasks

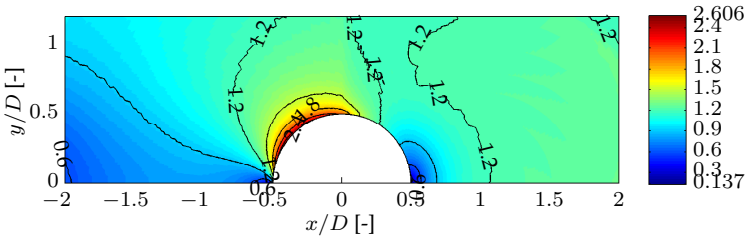

(a) Present (Brørs model)

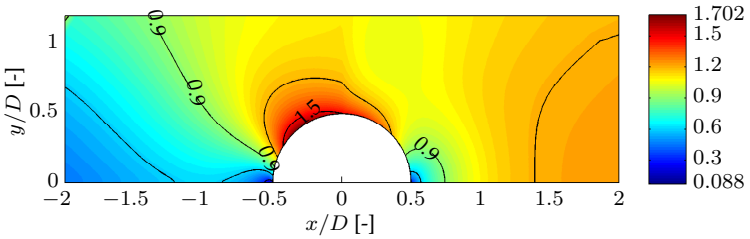

(b) Present (Roulund model)

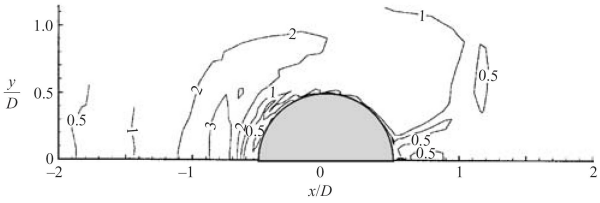

(c) Roulund et al. [2005]

Figure 5.6 *Bed shear stress amplification τ'/τ'_{ref} during current scouring.*

Current is coming from left.

of deriving recommendations for the sediment transport models, using the reverse approach for parametric studies of the time scale t_V, and generalize the approach further, say treating cases of combined current and waves.

A comparison was not possible in the case of waves due to the lack of studies for comparable configurations. The laminar oscillatory flow study of Umeda et al. [2008] treated Reynolds numbers up to $R_{\text{ref}} = U_{cu}D/\nu = 5 \cdot 10^3$ and reported the instantaneous bed shear stress for the case when $K = 20$ and horseshoe vortices were present. This is different from the present backfilling runs with $R_{\text{ref}} = 2 \cdot 10^4$, $K = 3$ and expected absence or short-lived horseshoe vortices as argued in Sec. 4.3.3. Nevertheless, I expect that the backfilling simulations of the reverse approach would agree better with corresponding flow studies because it would be reasonable to expect the maximum amplification in the oblique zone due to the side-flow as reviewed in Sec. 3.2.3. Here, the backfilling simulations of the reverse approach predict $\tau'/\tau'_{\text{ref}} \approx 1.4 - 2.4$ depending on the input parameters (see Sec. 7 of Ref. 4). For higher Keulegan-Carpenter numbers, the discrepancy is likely to manifest itself as horseshoe vortices become dominant. This latter outlook hampers the present use of the reverse approach for sufficiently high Keulegan-Carpenter numbers.

As the comparison in connection with Fig. 5.6 demonstrated, the inference from low-level input quantities to high-level response quantities that is performed in the reverse approach will likely be approximate and filtered to some degree in time and space. In itself, the filtering appears to be acceptable since the aim of the model is confined to provide estimates of filtered quantities rather than determine the instantaneous quantities. However, future research dealing with the above-mentioned discrepancy must demonstrate that the filter is not too brutal so as to prohibit any useful estimation.

On a final note, the *forward* approach also facilitates indicative parametric analyses when the field for the bed shear stress τ'_α is prescribed parametrically instead of being resolved from the transport equations. In such an approach, the suspended load model must be determined indirectly based on the bed shear stress instead of a transport equation for the grain concentration and the present model for sediment entrainment may prove valuable. Compared to the reverse approach, the use of a forward approach in this way would involve less assumptions but in turn requires more trials to obtain the targeted set of the scour depth rate and scour volume

rate. In this case, it remains an open question which of these approaches are preferable and both are encouraged.

* * *

Chapter 6

Conclusion & Future Work

In this chapter, the main conclusions of the present research and suggestions for future work are outlined.

6.1 Legacy I: Framework for Scour Geometry

1. Based on a review of how parameters are obtained, defined and related to the physical process, the combined use of the scour depth S and the scour volume V is recommended for scour forecasting.
2. The scour depth is retained because it can be obtained from a variety of bed measuring techniques, can be defined unambiguously, appears to be directly related to global sliding during scouring and allows a continuation based on existing research.
3. During backfilling, sliding can be less pronounced and the shape of the hole may change. Therefore, the scour depth cannot alone characterize the scour hole in general. The scour volume is favored rather than the scour length, scour breath or scour area because the scour volume is least sensitive to the exact location of the outer boundary. This boundary can be difficult to assert in practice during live-bed and model-scale conditions as relatively large bed forms appear. The scour volume also enjoys other advantages as given in Sec. 4.4.

4. The scour volume and scour depth at the same moment in time can be coupled through the definition of a scour shape factor ψ defined by $V \equiv \psi S^3$. If scour holes could develop geometrically similar, i.e. when all dimensions are scaled uniformly, the scour shape factor is constant with respect to time, i.e. $d\psi/dt = 0$, regardless of the shape of the scour hole. Scour holes can never develop perfectly geometrically similar but appear to do so approximately during most of the scouring process.
5. Based on the present experiments, the best fit to the scour depth and scour volume is obtained through a volume-based general approach. Here, the scour volume and scour shape factors are modeled with a set of simple ordinary differential equations, namely (4.15) and (4.16), and the scour depth is determined implicitly from these through the definition of the scour shape factor $S = (V/\psi)^{1/3}$.
6. A generalization of the equation of Sumer, Fredsøe and coworkers (3.1) leads to a scour depth equation (4.14) that fits well to the scour depth during scouring and some of the backfilling tests. However, the principal behavior of the equation conflicts with the measured scour depth development during backfilling for small holes, implying that the scour depth can be overestimated here.
7. Assuming that the scour holes develop geometrically similar during scouring from a plane bed, the results based on the generalized scour depth equation (3.1) or the scour volume equation (4.15) are shown to always give comparable results. This indicates strongly that the two equations share empirical basis during scouring. In this case, the time scale of the scour depth t_S and of the scour volume t_V are determined theoretically as $t_V/t_S \approx 2.4$. This relation can be used to estimate the time scale t_V in the scour volume equation based on existing scouring tests and e.g. the time scale formula (3.2). The depth-based similarity-approach also allows one to estimate the scour volume development but at a reduced accuracy in comparison with the scour volume equation.
8. The present framework entails some departure from the traditional focus of scouring tests that only deals with the development of the scour depth. In this framework, the scour volume

becomes equally important. The introduction of the scour volume also entails a change in bed measuring techniques from typically pile base imagery to bathymetry techniques.

9. The present experiments are unique in treating the temporal development during backfilling around a monopile and reporting the scour volume but also only treated a limited number of sea states and are impaired in some respects. Therefore, the present framework cannot be applied yet for scour forecasts.
10. Future experiments are encouraged to facilitate a more conclusive assessment of the present findings and provide calibration data for determining the parameter values of the modeled equations. These studies should treat scouring and backfilling at the present and a wider range of conditions and employ bathymetry techniques to obtain both the scour depth and scour volume.

6.2 Legacy II: The Reverse Approach

1. Laboratory or numerical studies of scouring and especially backfilling are time-consuming, can only investigate the influence of a limited number of parameters and are at present limited to model-scale. In contrast, the reverse approach is meant as a supplementary and indicative tool to do quicker and more comprehensive parametrical studies of the scouring and backfilling process. This can be used to estimate the time scale t_V that enters the scour volume equation.
2. The reverse approach relies on the interaction triangle that is traditionally used to couple the fluid flow, sediment transport and the bed surface. In the reverse approach, the point of departure is the bed surface and a prescribed scour geometry development given by the volume-based general approach. Using the same links as in a forward approach, the remaining items in the triangle are determined in a retrospective manner.
3. A new model is used for the suspended load in the interaction triangle. The entrainment correlation is postulated to be proportional to the product of the friction velocity associated with skin friction and the mean grain concentration in the bed load layer. This model can be used in general but is

particularly suited for the reverse approach because it simultaneously satisfies the conditions at equilibrium entrainment without requiring a transport equation for the grain concentration to be solved. The model lends further empirical support in the situation of equilibrium entrainment but has not been studied in more general situations.

4. A comparison between the simulations of the reverse approach and the flow results of Roulund et al. [2005] for a scoured bed subjected to steady current shows that the present simulations succeed in predicting the order of magnitude of the mean bed shear stress but fail to predict the intense amplification in the crescent-shaped zone upstream of the pile, presumingly due to presence of horseshoe vortices in the flow study. Until the discrepancy is resolved, parametric studies using the reverse approach are not recommended.
5. Future research is encouraged to:
    a) examine the suggested origins of the above-mentioned discrepancy to improve the prediction of the reverse approach for the case of current or high Keulegan-Carpenter waves.
    b) implement a parametrical forward approach so as to avoid some of the additional assumptions of the reverse approach.
    c) examine the turbulent flow around circular monopiles in scoured and rigid bed to allow further comparisons and provide calibration data. This is especially needed for the scarcely-treated case of waves.

* * *

Notes

Chapter 1: Context

1. When I refer to the wind turbine in gross terms, I characterize it by the power capacity of the generator since this is typically related to the mass and dimensions of the wind turbine.

2. By *support structure*, I mean the load-carrying structure that supports the tower – from the possible components embedded in the seabed, through those exposed to water to those above the water surface. This includes possible transition pieces and mooring devices but excludes secondary components such as platforms or pipes for cables. I refer to the central load-carrying component of the support structure as the *main support structure* if such an identification is possible. I refer to the tower and the support structure as a whole as the *total structure*.

Chapter 2: Aims

1. By *accurate* scour forecasts, I mean that the mapping from the parameters of the sea state to those of the scour geometry should minimize the difference between the *forecasted* and *measured* scour geometry. The latter refers loosely to the idealized representation that can be derived by measurement and ignores here the inherent uncertainties related to different measuring techniques and experimental set-ups. The difference should be within the error tolerance dictated by the application of the scour forecast. For rough estimates, higher error tolerances can usually be accepted.

Chapter 3: Review of Scour

1. Here, I have adopted the plural terminology of Dargahi [1989] rather than the singular one of Roulund et al. [2005], i.e. horseshoe *vortices* rather than horseshoe *vortex*. In my opinion, the first terminology conveys better that there are a multitude of vortices as demonstrated in e.g. Dargahi [1989] or Kirkil et al. [2008] although one may think or model them as a single vortex as an approximation.

2. The singular is used for the vortices at the free surface since this is simpler and the loss of clarity is permissible for these since they are only of indirect importance to scour.

3. This flow feature is usually referred to as *contraction of streamlines* in the line of work of Sumer et al. [1992b] but the present terminology is adopted to avoid the confusion that arises when streamlines elsewhere in the flow also contract as illustrated in Fig. 3.2.

4. Here, I note that there is an error in the description in Secs. 1–2 of Ref. 1, e.g. between Eqs. (5)-(6), stating erroneously that the experiments were conducted by scouring a plane bed with current and then subsequently backfilled by superimposed waves. The present description is correct.

Chapter 5: Legacy II: The Reverse Approach

1. One of the largest wave flumes worldwide is the Large Wave Channel (Grosser WellenKanal, GWK) of Coastal Research Center (Forschungszentrum Küste) in Hannover, Germany. The wave flume is 7.00 m deep, $W = 5.00\ \mathrm{m}$ wide and 307 m long. Wave heights can be up to 2.00 m and the water depth up to $H = 5\ \mathrm{m}$ [Oumeraci, 2010, Hydralab]. A notable flume for steady current is the Water Soil Flume of Deltares in Netherlands. The main flume is 2.5 m deep, $W = 5.5\ \mathrm{m}$ wide and can be up to 50 m long. The water depth can be up to $H = 2.5\ \mathrm{m}$ [Hydralab]. If we require $W/D = 7$ for flow clearance for the pile and the scour hole and take $D = 5\ \mathrm{m}$ to be representative for field-scale monopiles for offshore

wind parks, the dimensions of these flumes allow scaling ratios of about 1:7.

2. The flow around a field-scale monopile is expected to be predominantly turbulent with massive separation occurring at the bed and/or at the pile. The boundary layers here are expected to play an important role in influencing lines of separation, the downflow and thus also the larger horseshoe or wake vortices. Therefore, the extremely fine turbulence in the boundary layers must ideally be resolved and treated down to the Kolmogorov length scale, say one tenth of the wall unit length scale, by a direct-numerical-simulation (DNS) technique or down to the wall unit length scale by the large-eddy-simulation (LES) technique. As an approximation, the turbulence in the boundary layers can be modeled but the mean flow across the thin thickness of the boundary layers must still be resolved, say with 10 cells, as in classical Reynolds-averaged methods or detached eddy-simulations (DES). In either case, the requirements for the spatial resolution and thus also the temporal resolution due to the Courant condition are immense. If we take the recent LES and DES studies of Kirkil et al. [2008, 2009] as yardsticks for present computational capabilities, they treated a pile diameter of $D = 0.09\ \mathrm{m}$ and $D = 0.46\ \mathrm{m}$, respectively. The latter case can be field-scale for some bridge piles but remains model-scale for the monopiles of offshore wind parks with a scaling ratio of about 1:11.

* * *

Bibliography

S. Baglio, C. Faraci, E. Foti, and R. Musumeci. Measurements of the 3-d scour process around a pile in an oscillating flow through a stereo vision approach. *Measurement*, 30(2):145 – 160, 2001. ISSN 0263-2241. doi: 10.1016/S0263-2241(00)00064-6.

R. A. Bagnold. Experiments on a gravity-free dispersion of large solid spheres in a newtonian fluid under shear. In *Proc. Royal Society of London. Series A, Mathematical and Physical Sciences*, volume 225, pages 49–53. Royal Society, 1954.

C.J. Baker. The turbulent horseshoe vortex. *J. Wind Eng. and Industrial Aerodynamics*, 6(1-2):9 – 23, 1980. ISSN 0167-6105. doi: 10.1016/0167-6105(80)90018-5.

J. Bakker. Foundation design monopile, variation of water depth and pile diameter, 3.6 & 6.0 mw wind turbines. Technical report, Ballast Nedam Engineering, 2003. Report no. 100130.R02 rev. A.

Francesco Ballio and Alessio Radice. A non-touch sensor for local scour measurements. *J. Hydraulic Research*, 41(1):105–108, 2003.

Francesco Ballio, Alessio Radice, and Subhasish Dey. Temporal scales for live-bed scour at abutments. *J. Hydraulic Eng.*, 136 (7):395–402, 2010. ISSN 07339429. doi: 10.1061/(ASCE)HY.1943-7900.0000191.

Abdul Karim Barbhuiya and Subhasish Dey. Local scour at abutments: A review. *Sadhana*, 29(5):449–476, 2004.

Filippo Bressan, Francesco Ballio, and Vincenzo Armenio. Turbulence around a scoured bridge abutment. *J. Turbulence*, 12(3):1–24, 2011. doi: 10.1080/14685248.2010.534797.

B. Brørs. Numerical modeling of flow and scour at pipelines. *J. Hydraulic Eng.*, 125(5):511–523, 1999. ISSN 0022-1120. doi: 10.1061/(ASCE)0733-9429(1999)125:5(511).

Y.M. Chiew. *Local scour at bridge piers*. PhD thesis, Department of Civil Engineering, Auckland University, 1984.

Danish Wind Industry Association. Vind på havet. In *Annoncetillæg til Jyllands-Posten (5 Dec 2011)*, 2011. URL www.windpower.org. In Danish (English title: Wind on the ocean. Add-in for the Jutland Post).

B. Dargahi. The turbulent flow field around a circular cylinder. *Experiments in Fluids*, 8:1–12, 1989. ISSN 0723-4864. doi: 10.1007/BF00203058.

Det Norske Veritas. Design of offshore wind turbine structures, June 2004. DNV-OS-J101.

Subhasish Dey and Abdul Karim Barbhuiya. Time variation of scour at abutments. *J. Hydraulic Eng.*, 131(1):11–23, 2005. doi: 10.1061/(ASCE)0733-9429(2005)131:1(11).

Subhasish Dey and Koustuv Debnath. Sediment pickup on streamwise sloping beds. *J. Irrigation and Drainage Eng.*, 127(1):39–43, 2001. doi: 10.1061/(ASCE)0733-9437(2001)127:1(39).

Subhasish Dey, B. Mutlu Sumer, and Jørgen Fredsøe. Control of scour at vertical circular piles under waves and current. 132(3):270–279, 2006. ISSN 07339429. doi: 10.1061/(ASCE)0733-9429(2006)132:3(270).

M. Rodríguez y Domínguez, R. Romero-Méndez, M. Ramos-Paláu, and F. G. Pérez-Gutiérrez. The laminar horseshoe vortex upstream of a short-cylinder confined in a channel formed by a pair of parallel plates. *J. Visualization*, 9(3):309–318, 2006.

Energistyrelsen. Kortlægning af bølgeenergiforhold i den danske del af nordsøen. Technical report, Energistyrelsen, 1999. Report no. 51191/97-0014. In Danish (English title: Mapping of wave energy resource in the Danish part of the North Sea).

Frank Engelund and Jørgen Fredsøe. A sediment transport model for straight alluvial channels. *Nordic Hydrology*, 7(5):293–306, 1976.

C. Faraci, E. Foti, and S. Baglio. Measurements of sandy bed scour processes in an oscillating flow by using structured light. *Measurement*, 28(3):159 – 174, 2000. ISSN 0263-2241. doi: 10.1016/S0263-2241(00)00009-9.

Jørgen Fredsøe. Turbulent boundary layer in wave?current motion. 110(8):1103–1120, 1984. ISSN 07339429. doi: 10.1061/(ASCE)0733-9429(1984)110:8(1103).

Jørgen Fredsøe and Rolf Deigaard. *Mechanics of coastal sediment transport*, volume 3 of *Advances series on Ocean Eng.* World Scientific, 1992. ISBN 981-02-0840-5.

Marcelo Garcia and Gary Parker. Entrainment of bed sediment into suspension. *J. Hydraulic Eng.*, 117(4):414–435, 1991. doi: 10.1061/(ASCE)0733-9429(1991)117:4(414).

Garden State Offshore Energy. Photos, Sep 2011. URL www.gardenstatewind.com. Accessed on 19 Sep 2010.

William K. George. Is there a universal log law for turbulent wall-bounded flows? In *Proc. Philosophical Transactions of Royal Society (series A)*, volume 365 of *A*, pages 789–806, 2007. doi: 10.1098/rsta.2006.1941.

S Gough. River geomorphology videos. DVD, 2007. URL www.emriver.com. Accessed on 19 Sep 2010.

R. Halfschepel. Concept study bottom protection around pile foundation of 3mw turbine. Technical report, Van Oord ACZ, 2001. Report no. DOWEC-F1W1-RH-01-023/02.

R. Halfschepel. Scour protection for 6mw owec with foundation in north sea. Technical report, Van Oord ACZ, 2003. Report no. DOWEC-F1W1-RH-02-050/01.

Peres Akrawi Hartvig. New framework for geometry of transient monopile scour. Presentation at 3rd workshop on Seabed Windfarm Interaction, November 2010.

Peres Akrawi Hartvig. Model for the evolving bed surface around an offshore monopile. In review, 2011a.

Peres Akrawi Hartvig. The reverse approach for monopile scour. Submitted, 2011b.

Peres Akrawi Hartvig, Jess McCann Thomsen, Peter Frigaard, and Thomas Lykke Andersen. Experimental study of the development of scour & backfilling. *Coastal Eng. J.*, 52(2):157–194, 2010. doi: 10.1142/S0578563410002154. Postprint available at vbn.aau.dk.

Peres Akrawi Hartvig, Jess McCann Thomsen, Peter Frigaard, and Thomas Lykke Andersen. Full erratum for "experimental study of the development of scour & backfilling". In *DCE Technical Memorandum*, number 12. Department of Civil Eng., Aalborg University, 2011. Available at vbn.aau.dk.

Hydralab. Hydralab facilities. URL www.hydralab.eu/facilities_interface.asp. Accessed on 19 Sep 2010.

Morten Sand Jensen, Brian Juul Larsen, Peter Frigaard, Leen De Vos, Erik D. Christensen, Erik Asp Hansen, Tron Solberg, Bjørn H. Hjertager, and Stefano Bove. Offshore wind turbines situated in areas with strong currents. Technical report, Offshore Center Danmark, 2006. URL vbn.aau.dk. Report no. 6004RE01ER1.

J. Jonkman, S. Butterfield, W. Musial, and G. Scott. Definition of a 5-mw reference wind turbine for offshore system development. Technical report, National Renewable Energy Laboratory, 2009. Report no. NREL/TP-500-38060.

G. Kirkil, S. G. Constantinescu, and R. Ettema. Coherent structures in the flow field around a circular cylinder with scour hole. *J. Hydraulic Eng.*, 134(5):572–587, 2008. ISSN 07339429. doi: 10.1061/(ASCE)0733-9429(2008)134:5(572).

G. Kirkil, G. Constantinescu, and R. Ettema. Detached eddy simulation investigation of turbulence at a circular pier with scour hole. *J. Hydraulic Eng.*, 135(11):888–901, 2009. ISSN 07339429. doi: 10.1061/(ASCE)HY.1943-7900.0000101.

Gokhan Kirkil, George Constantinescu, and Robert Ettema. The horseshoe vortex system around a circular bridge pier on equilibrium scoured bed. In P.E Raymond Walton, editor, *Proc. World*

Water and Environmental Resources Congress, volume 173, pages 414–414. ASCE, 2005. ISBN 0-7844-0792-4. doi: DOI:10.1061/40792(173)414.

Tomonao Kobayashi. 3-d analysis of flow around a vertical cylinder on a scoured bed. In Billy L. Edge, editor, *Proc. 23rd International Conference on Coastal Eng. (Venice)*, pages 3482–3495. ASCE, 1992. ISBN 0-87262-933-3.

Lindoe Offshore Renewables Center. Knowledge, offshore renewables map, Sep 2011. URL www.lorc.dk/knowledge. Accessed on 19 Sep 2010.

Oscar Link. Time scale of scour around a cylindrical pier in sand and gravel. In *Proc. 3rd Chinese-German Joint Symposium on Coastal and Ocean Eng.*, 2006a.

Oscar Link. *Untersuchung der Kolkung an einem schlanken zylindrischen Pheiler in sandigem Boden*. PhD thesis, Institut für Wasserbau und Wasserwirtschaft, Technische Universität Darmstadt, 2006b. Heft 136.

Oscar Link and Ulrich Zanke. On the time-dependent scour-hole volume evolution at a circular pier in uniform coarse sand. In *Proc. 2nd International Conference on Scour and Erosion (ICSE), Singapore*, 2004.

Xiaofeng Liu and Marcelo H. García. Three-dimensional numerical model with free water surface and mesh deformation for local sediment scour. *J. Waterway, Port, Coastal and Ocean Eng.*, 134(4): 203–217, 2008. doi: 10.1061/(ASCE)0733-950X(2008)134:4(203).

Matthew Lueker, Jeff Marr, Chris Ellis, Vincent Winsted, and Shankar Reddy Akula. Bridge scour monitoring technologies: Development of evaluation and selection protocols for application on river bridges in minnesota. Technical report, Minnesota Department of Transportation, 2010. Report no. MN/RC 2010-14.

B. W. Melville and A. J. Sutherland. Design method for local scour at bridge piers. 114(10):1210–1226, 1988. ISSN 07339429. doi: 10.1061/(ASCE)0733-9429(1988)114:10(1210).

Bruce W. Melville and Yee-Meng Chiew. Time scale for local scour at bridge piers. *J. Hydraulic Eng.*, 125(1):59–65, 1999. ISSN 0733-9429/99/0001-00590065.

E. Meyer-Peter and R. Müller. Formulas for bed-load transport. In *Proc. International Association for Hydraulic Structures Research (2nd Meeting)*, pages 39–64. Oskar Eklunds Boktryckeri, Stockholm, Sweden, 1948.

National Association for Better Environment, Sep 2011. URL www.nationalttestcenter.dk. Accessed on 19 Sep 2010.

Peter Nielsen. *Coastal bottom boundary layers and sediment transport*, volume 4 of *Advances series on Ocean Eng.* World Scientific, 1992. ISBN 981-02-0472-8.

J. C. Oud. Foundation design monopile, comparison extra steel consumption versus scour protection, 3.6 & 6.0 mw wind turbines. Technical report, Ballast Nedam Engineering, 2003. Report no. 100130.R03.

Hocine Oumeraci. Selected research projects using the grosser wellenkanal (gwk). In *Proc. Workshop of the Celebration of 60th Anniversary of Tainan Hydraulic Laboratory*, 2010.

T.U. Petersen and L. Locatelli. Backfilling process for offshore wind farms. Master's thesis, Technical University of Denmark (DTU), 2010.

Tim Raaijmakers and Daniel Rudolph. Time-dependent scour development under combined current and waves conditions - laboratory experiments with online monitoring technique. In *Proc. 4th International Conference on Scour and Erosion (ICSE)*, pages 152–161, 2008.

Rambøll. Services for offshore wind energy, Sep 2011. URL www.ramboll.com/wind. Accessed on 19 Sep 2010.

Leo C. van Rijn. Sediment transport, part ii: Suspended load transport. *J. Hydraulic Eng.*, 110(11):1613–1641, 1984b. ISSN 0733-9429/84/0011-1613. doi: 10.1061/(ASCE)0733-9429(1984)110:11(1613). URL www.leovanrijn-sediment.com.

Leo C. van Rijn. Sediment pick-up functions. *J. Hydraulic Eng.*, 110 (10):1494–1502, 1984d. doi: 10.1061/(ASCE)0733-9429(1984)110:10(1494). URL www.leovanrijn-sediment.com.

Leo C. van Rijn. Mathematical models for sediment concentration profiles in steady flow. In *Transport of Suspended Solids in Open Channels: Proc. Euromech 192 (Munich)*, 1985. URL www.leovanrijn-sediment.com.

Andreas Roulund. *Three-dimensional numerical modelling of flow around a bottom-mounted pile and its application to scour*. PhD thesis, Technical University of Denmark (DTU), Denmark, 2000.

Andreas Roulund, B. Mutlu Sumer, Jørgen Fredsøe, and Jess Michelsen. Numerical and experimental investigation of flow and scour around a circular pile. *J. Fluid Mechanics*, 534:351–401, 2005. ISSN 0022-1120. doi: 10.1017/S0022112005004507.

Søren Peder Hyldal Sørensen, Lars Bo Ibsen, and Peter Frigaard. Experimental evaluation of backfill in scour holes around offshore monopiles. In Søren A. Nielsen, editor, *Program Review, July 2009 - June 2010*. MBD Offshore Power A/S and Aalborg University, 2010.

B. M. Sumer, N. Christiansen, and J. Fredsøe. Influence of cross section on wave scour around piles. *J. Waterway, Port, Coastal and Ocean Eng.*, 119(5):477–495, 1993. ISSN 0733950X. doi: 10.1061/(ASCE)0733-950X(1993)119:5(477).

B. M. Sumer, N. Christiansen, and J. Fredsøe. The horseshoe vortex and vortex shedding around a vertical wall-mounted cylinder exposed to waves. *J. Fluid Mechanics*, 332:41–70, 1997.

B. Mutlu Sumer and Jørgen Fredsøe. *Hydrodynamics around cylindrical structures*. World Scientific, reprint edition, 1997. ISBN 981-02-2898-8.

B. Mutlu Sumer and Jørgen Fredsøe. Scour around pile in combined waves and current. *J. Hydraulic Eng.*, 127(5):403–411, 2001. ISSN 07339429. doi: 10.1061/(ASCE)0733-9429(2001)127:5(403).

B. Mutlu Sumer and Jørgen Fredsøe. *The Mechanics of scour in the marine environment*, volume 17 of *Advances series on Ocean Eng.* World Scientific, 2002. ISBN 981-02-4930-6.

B. Mutlu Sumer, Lloyd H. C. Chua, N.-S. Cheng, and Jørgen Fredsøe. Influence of turbulence on bed load sediment transport. *J. Hydraulic Eng.*, 129(8):585–596, 2003. ISSN 0733-9429/2003/8-585596. doi: 10.1061/(ASCE)0733-9429(2003)129:8(585).

B. Mutlu Sumer, Figen Hatipoglu, and Jørgen Fredsøe. Wave scour around a pile in sand, medium dense, and dense silt. 133(1):14–27, 2007. ISSN 0733950X. doi: 10.1061/(ASCE)0733-950X(2007)133:1(14).

B.M. Sumer, N. Christiansen, and J. Fredsøe. Time scale of scour around a vertical pile. In *Proc. 2nd International Offshore and Polar Eng. Conference (San Francisco)*, volume 3, 1992a. ISBN 1-880653-03-6.

B.M. Sumer, J. Fredsøe, and N. Christiansen. Scour around vertical pile in waves. *J. Waterway, Port, Coastal and Ocean Eng.*, 118(1): 15–31, 1992b. ISSN 0733-950X/92/0001-0015.

Jess McCann Thomsen. Scour in a marine environment. Master's thesis, Aalborg University, 2006. URL `projekter.aau.dk`.

Shinya Umeda, Masatoshi Yuhi, and Hajime Ishida. Numerical study of three-dimensional flow fields around the base of a vertical cylinder in oscillatory plus mean flow. In *Proc. Coastal Structures 2003*, volume 147, pages 751–763. ASCE, 2003. doi: 10.1061/40733(147)62.

Shinya Umeda, Liang Cheng, Masatoshi Yuhi, and Hajime Ishida. Three-dimensional numerical model of flow and scour around a vertical cylinder. In Jane McKee Smith, editor, *Proc. 30th International Conference of Coastal Eng.*, volume 3, pages 2354–2366. World Scientific, 2006. doi: 10.1142/9789812709554_0199.

Shinya Umeda, Masatoshi Yuhi, and Hajime Ishida. Three-dimensional numerical model for wave-induced scour around a vertical cylinder. In Jane McKee Smith, editor, *Proc. 31st International Conference of Coastal Eng. (Hamburg)*, pages 2717–2729. World Scientific, 2008. doi: 10.1142/9789814277426_0224.

J. Unger and W. H. Hager. Down-flow and horseshoe vortex characteristics of sediment embedded bridge piers. *Experiments in Fluids*, 42:1–19, 2007. doi: 10.1007/s00348-006-0209-7.

Richard J. S. Whitehouse. *Scour at marine structures: A manual for practical applications*. Thomas Telford Publications, 1998. ISBN 0-7277-2655-2.

Richard J.S. Whitehouse, John M. Harris, James Sutherland, and Jon Rees. The nature of scour development and scour protection at offshore windfarm foundations. *Marine Pollution Bulletin*, 62(1):73 – 88, 2011. ISSN 0025-326X. doi: 10.1016/j.marpolbul.2010.09.007.

M. Yuhi, H. Ishida, and S. Umeda. A numerical study of three-dimensional flow fields around a vertical cylinder mounted on a bed. In I. J. Losada, editor, *Proc. International Conference Coastal Structures '99*, pages 783–792. Balkema Publishers, 2000. ISBN 90-5809-092-2.

M.B. Zaaijer and J. Van der Templ. Scour protection: a necessity or a waste of money? In *Proc. 43rd IEA Topical Expert Meeting on Critical Issues Regarding Offshore Technology and Deployment (Skaerbaek, Denmark)*, pages 43–51, 2004.

M.B. Zaaijer, W. van den Broek, and G.J.W. van Bussel. Toward selection of concepts for offshore support structures for large scale wind turbines. In *Proc. Marine Renewable Energy Conference (MAREC), Newcastle*, 2001.

Wei Zhao and Aode Huhe. Large-eddy simulation of three-dimensional turbulent flow around a circular pier. *J. Hydrodynamics*, 18(6):765–772, 2006. doi: 10.1016/S1001-6058(07)60019-5.

* * *

Part II

References

The publications have been omitted from this electronic version due to copyright restrictions. The publications may be availible at Aalborg University's electronic repository: http://vbn.aau.dk.